Molecular engineering of ionic organic phototheranostic agents for NIR-II imaging-guided synergistic phototherapy

Jianye Gong[1,†], Yue Zhang[1,†], Chen Lu[1], Guoyu Jiang[1,*], Quan Jin[1,*] and Jianguo Wang[1,*]

1 J. Gong, Y. Zhang, C. Lu, Prof. G. Jiang, Q. Jin, Prof. J. Wang
College of Chemistry and Chemical Engineering, College of Green Chemistry and Environment, Institutes of Biomedical Sciences
Inner Mongolia Key Laboratory of Synthesis and Application of Organic Functional Molecules
Inner Mongolia University
Hohhot 010021, P. R. China
E-mail: jiangguoyu@mail.ipc.ac.cn quanjin620@163.com wangjg@iccas.ac.cn

† Equally contributed to this work.

Experimental procedures

Materials

Phosphate buffered solution (PBS, 10 mM, pH 7.4), and 9,10-anthracenediyl-bis(methylene) dimalonic acid (ABDA) were purchased from Sigma-Aldrich. Thiazolyl blue tetrazolium bromide (MTT) was purchased from Beyotime biotechnology Co., Ltd. All other chemicals and reagents were purchased from Admas-beta® and used directly without further purification.

Instruments

^{1}H and ^{13}C NMR spectra were recorded with Bruker ARX 600 NMR spectrometer using tetramethylsilane (TMS) as a reference. High resolution mass spectra (HRMS) were measured with a LCMS9030 spectrometer. UV-vis absorption spectra were recorded on a SHIMADZU UV-2600i spectrophotometer. Photoluminescence (PL) spectra were recorded on a FS5 fluorescence spectrophotometer. Temperature change was monitored by an FLIR E8-XT camera (FLIR System). Photodynamic and photothermal experiments were conducted using a 660 nm laser (CNI laser, MDL-XD-660) as the excitation light source. The cell viability was assessed by MTT assay, and the absorbance of each sample was measured at 490 nm using a microplate reader (BioTek). The *in vivo* fluorescence images were acquired on the commercial NIR-II Small Animal Imaging System Series III 900/1700S (Suzhou NIR-Optics Technology Co., Ltd., China) equipped with 900 nm long-pass (LP) filters. The blood biochemistry parameters were collected by the fully automatic biochemical analysis (Chemray 240).

Fluorescence Quantum Yield (QY)

The relative fluorescence quantum yield of the four ionic OPTAs in DMSO or in aqueous solution was calculated by standard method using ICG (QY: 2.7 %) as the reference.[1,2] Upon 660 nm laser irradiation, the fluorescence spectra of the four ionic OPTAs with different absorption intensity (0.02, 0.04, 0.06, 0.08, 0.10) at 660 nm were recorded. The obtained emission spectra were integrated ranging from 700-1300 nm. The obtained integrated fluorescence intensity was plotted vs. absorption intensity at 660 nm. The QY of the four ionic OPTAs were calculated according to equation (a):

$$QY_{sample} = QY_{ref} \times \frac{slope_{sample}}{slope_{ref}} \times \left(\frac{n_{sample}}{n_{ref}}\right)^2 \quad \text{(a)}$$

where QY_{sample} is the QY of OPTAs with a wavelength of 700-1300 nm, QY_{ref} is the QY of ICG, $slope_{sample}$ is the slope obtained by linear fitting of the integrated fluorescence intensity of OPTAs with a wavelength of 700-1300 nm against the absorption intensity at 660 nm, $slope_{ref}$ is the slope obtained by linear fitting of the integrated fluorescence intensity of ICG with a wavelength of 700−1300 nm against the absorption intensity at 660 nm, n_{sample} and n_{ref} are the refractive indices of water (1.333) or DMSO (1.47).

$^1O_2$ Detection by ABDA

A commonly used $^1O_2$ indicator ABDA was utilized to detect the $^1O_2$ generation of the four ionic OPTAs in PBS under 660 nm laser irradiation (0.1 W cm^{-2}). Briefly, ABDA (40 μL, 50 μM) in PBS and the ionic OPTAs (1 μM) was added to PBS for monitoring the UV-vis absorption spectra of ABDA at different time intervals to indicate the $^1O_2$ generation.

•OH Detection by APF

The •OH generation measurements were performed using aminophenyl fluorescein (APF) as an indicator. The stock solution of APF (5 mM) was diluted to 5 μM in the sample solution of the ionic OPTAs (1 μM) in PBS. The fluorescence signal of APF was monitored at different time intervals in a range of 500-600 nm with the excitation wavelength at 480 nm after the solution was irradiated by 660 nm laser irradiation (0.1 W cm^{-2}). The fluorescence intensity at 517 nm was recorded to indicate the •OH generation rate of the ionic OPTAs.

$O_2^{\bullet-}$ Detection by DHR123

The $O_2^{\bullet-}$ generation measurements were performed using dihydrorhodamine 123 (DHR123) as an indicator. The stock solution of DHR 123 (1 mM) was diluted to 1 μM in the sample solution of the ionic OPTAs (1 μM) in PBS. The fluorescence signal of DHR 123 was monitored at different time intervals in a range of 500-600 nm with the excitation wavelength at 490 nm after the solution was irradiated by 660 nm laser irradiation (0.1 W cm^{-2}). The fluorescence intensity at 528 nm was recorded to indicate the $O_2^{\bullet-}$ generation rate of the ionic OPTAs.

Photothermal Properties

The solution containing one of the OPTAs (60 μM) was irradiated by 660 nm laser at different power densities (0.1 W cm^{-2}, 0.2 W cm^{-2}, 0.3 W cm^{-2} and 0.4 W cm^{-2}). The temperature changes were monitored by FLIR E8-XT camera. Different concentrations of the ionic OPTAs were prepared (0 μM, 5 μM, 10 μM, 20 μM and 60 μM), and irradiated by 660 nm laser (0.4 W cm^{-2}) for 6 min. The temperature changes were monitored during irradiation. The photothermal conversion efficiency of NPs was determined according to previously reported publications.[3] The solution of the ionic OPTAs (60 μM) were exposed to 660 nm laser irradiation at 0.4 W cm^{-2} for 6 min when the temperature reached a plateau. At this time point, the laser was shut off. Then the solution was cooled down to room temperature. The temperature of the solution was recorded at an interval of 15 s during this process. The photothermal conversion efficiency was determined according to Equation (b), and the other parameters in equation (b) were calculated from equation (c), (d) and (e).

$$\eta = \frac{hS(T_{Surr}T_{Max} -) - Q_{Dis}}{I(1 - 10^{-A_{660}})} \quad \text{(b)}$$

$$\tau_s = \frac{\sum_i m_i C_{p,i}}{hS} \quad \text{(c)}$$

$$t = \tau_s(-ln\,\theta) \quad \text{(d)}$$

$$\theta = \frac{T - T_{Surr}}{T_{Max} - T_{Surr}} \quad \text{(e)}$$

In equation (a), η is the photothermal conversion efficiency, *h* is the heat transfer coefficient; *S* is the surface area of the container. Q_{dis} represents heat dissipated from the laser mediated by the solvent and container. *I* is the laser power and A_{660} is the absorbance of the sample at 660 nm. In equation (b), *m* is the mass of the solution containing the photoactive material, *C* is the specific heat capacity of the solution (C_{water} = 4.2 J g^{-1}). In equation (c), τ_s is the associated time constant. In equation (d), θ is a dimensionless parameter, known as the driving force temperature. T_{max} and T_{Surr} are the maximum steady state temperature and the environmental temperature, respectively.

Cell Culture

HeLa, LO2 and 4T1 cells were cultured in DMEM medium (containing 10% heat-inactivated FBS, 1% 100 mg·mL^{-1} penicillin and 100 mg·mL^{-1} streptomycin) at 37 °C in a humidified incubator with 5% CO_2. Before the experiments, the cells were precultured until confluence was reached. For the imaging, the HeLa cells were incubated with 2PyI at 37 °C. The imaging was acquired using an inverted fluorescent microscope. Then, the cells were washed with PBS three times. A 426−490 nm laser was used as the light source and emission after 550−641 nm was collected.

Cell Viability

HeLa, LO2 or 4T1 cells in a logarithmic growth phase were seeded on 96-well plates in DMEM medium (with 10% FBS, 1% penicillin/streptomycin) at a density of 5 × 10^3 cells for 24 h incubation in 5% CO_2, 20% O_2 at 37 °C in a humidified incubator. Subsequently, the medium was replaced with the fresh medium containing different concentrations of ionic OPTAs. After further incubation for 20 h, the cells were exposed to 660 nm laser irradiation (0.4 W cm^{-2}) for 10 min. Meanwhile, the OPTAs-incubated cells without laser irradiation were also conducted for the dark cytotoxicity study. After further incubation for 4 h, MTT (10 μL, 5 mg/mL) was added and cells were incubated for another 4 h in the dark. Finally, the absorbance of the products was measured at a wavelength of 490 nm by a microplate reader. The results were expressed as the viable percentage of cells after different treatments relative to the control cells without any treatment. The relative cell viability was calculated according to the following formula:

$$\text{Cell viability (\%)} = (OD_{sample} - OD_{background})/(OD_{control} - OD_{background}) \times 100\% \quad \text{(f)}$$

Live/Dead Cell Staining Assay

First, HeLa and 4T1 cells were seeded on 6-well plate at a density of ~10^5 cells per well and cultured in incubator for 24 h. Then, remove the old media and replace it with fresh DMEM containing PBS or 2PyI (5 μM). After 20 h, the cells were subjected to dark or laser treatment (laser applied: 660 nm, 0.4 W cm^{-2}, 10 min). After the treatment, the cells were rinsed with PBS and stained by using 1 μM Calcein-AM and 1 μM PI for 30 min. The residual dyes were washed out by PBS for three times. The inverted fluorescent microscope was applied to observe the green fluorescence of Calcein-AM and red fluorescence of PI indicating live and dead cells, respectively. Conditions: excitation wavelength: 426-466 nm for Calcein-AM, 500-550 nm for PI; emission filter: 511-551 nm for Calcein-AM, 573-613 nm for PI.

Tumor Xenograft Model and Imaging

BALB/c mice (6−8 weeks old, average body weight 16−18 g) were purchased from SPF Biotechnology Co., Ltd. (Beijing, China). All procedures were approved by the Institutional Animal Care and Use Committee at the Inner Mongolia University (IMU-2023-mouse-017). All animals were acclimatized to the animal facility for one week prior to experimentation and housed under pathogen-free conditions, fed under conditions of 25 °C and 55% of humidity and allowed free access to standard laboratory water and chow. To establish the 4T1 tumor-bearing mouse models, 4T1 breast cancer cells (1 × 10^6) suspended in 100 μL PBS were injected subcutaneously into the right flanks of each mouse. After about 7 days, mice with tumor volumes at about 100 mm^3 were used subsequently. The 4T1 tumor-bearing mice were administered with 2PyI or ICG (1 mM, 100 μL) through intratumoral injection. Then, the fluorescence images of mice were obtained as a function of post injection times (0, 4, 8, 12, 24, 48, 72 h) with 900 nm long-pass filter.

Phototheramal Imaging

The 4T1 tumor-bearing BALB/c mice were intravenously injected with 2PyI (1 mM, 100 μL). The infrared thermal images of mice were acquired by using an FLIR E8-XT camera with 660 nm laser (0.5 W cm^{-2}) irradiation for 10 min at 48 h after administration of 2PyI. Mice injected with PBS under the same irradiation condition were used as the control.

In Vivo Synergistic Photodynamic and Photothermal Cancer Therapy

The 4T1 tumor-bearing BALB/c mice were randomly divided into 4 groups (n = 4 for each group), which were named “PBS”, “PBS+L”, “2PyI” and “2PyI+L”, respectively. For “PBS” and “2PyI” groups, 100 μL of PBS or 2PyI (1 mM) were intratumorally injected into the mice, respectively, without further laser irradiation. While for “PBS+L” and “2PyI+L” groups, the mice were further irradiated by 660 nm laser (0.5 W cm^{-2}) for 10 min at 48 h post-injection of PBS or 2PyI, respectively. Tumor volumes were measured and calculated every other day using a caliper and calculated using the following formula:

$$\text{volume} = ((\text{tumor length}) \times (\text{tumor width})^2)/2 \qquad (g)$$

Histological Examination

After 12 days of treatment, the mice of various groups (“PBS”, “PBS+L”, “2PyI” and “2PyI+L”) were sacrificed for further haematoxylin-eosin (H&E) staining on tumor tissues and normal organs (heart, liver, spleen, lung, and kidneys).

Biosafety Evaluation

To further evaluate the safety of different treatments *in vivo*, blood samples were collected from mice with various treatments for complete blood panel analysis. Red blood cell (RBC), hemoglobin (HGB), hematocrit (HCT), mean corpuscular volume (MCV), mean corpuscular hemoglobin (MCH), mean corpuscular hemoglobin concentration (MCHC), plateletocrit (PCT), platelet distribution width (PDW) and mean platelet volume (MPV) were measured. For biochemical blood analysis, alanine aminotransferase (ALT), transaminase (AST), albumin (ALB), urea (UREA), creatinine (CREA) and uric acid (UA) were measured.

Hemolysis Test

The erythrocytes were obtained by centrifuging the mouse blood (2000 rpm, 10 min). PBS was used to wash the obtained erythrocytes for three times, and then the purified erythrocytes were further diluted to a final concentration of 5% (*v*/*v*) with 0.1% Triton x-100 (1 mL) as positive group, PBS buffer (1 mL) as negative group and PBS buffer containing 5, 10, 20, 30 μM of 2PyI (1 mL) as experimental samples. Then, all the samples were shaken in an incubator at 37 °C for 1 h with a shaking speed of 100 rpm. After that, the microplate well contents were centrifuged (at 2000 rpm) for 10 min and the supernatant (100 μL) was then added into a new 96-well microplate. The absorbance of the solution was read at 540 nm by a microplate reader (Biotek). The hemolysis percentage was calculated from the following formula: Hemolysis rates = (sample absorbance-negative absorbance)/(positive absorbance-negative absorbance)×100%.

Statistical Analysis

All data were expressed in this article as mean result ± standard deviation (s.d.). All figures shown in this article were obtained from three or more independent experiments with similar results unless specific mention. The statistical significance of differences between groups was determined by using the unpaired-sample t test in SPSS 23 software. A value of $P < 0.05$ was considered to indicate significance and is indicated with asterisks: $*p < 0.05$, $**p < 0.01$ and $***p < 0.001$.

Synthesis and characterization

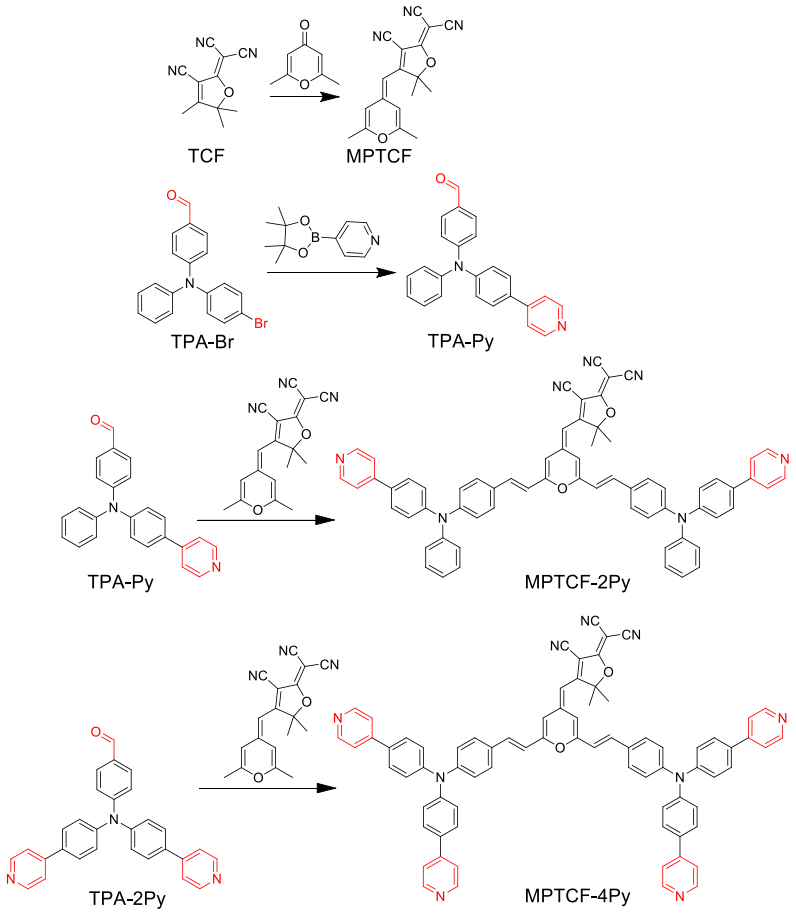

Scheme S1. Synthetic routes to compounds MPTCF-2Py and MPTCF-4Py.

Synthesis of MPTCF: To a 100 mL flask was added TCF (597.6 mg, 3.0 mmol), 2,6-dimethyl-4*H*-pyran-4-one (1117.3 mg, 9.0 mmol) and acetic anhydride (3.0 mL). The mixture was stirred at 110 °C under an atmosphere of N_2 for 12 h. After the reaction was completed, the mixture was cooled to room temperature. Saturated Na_2CO_3 aqueous solution was added to neutralize the residual acetic anhydride. Then the resulting mixture was extraceted with CH_2Cl_2 and washed with saturated aq. NaCl. The organic layer was collected, dried over Na_2SO_4, filtered, and concentrated under reduced pressure. The crude product was purified by silica gel column chromatography using CH_2Cl_2 as an eluent. Finally, recrystallization using CH_2Cl_2/hexane afforded the target compound MPTCF as a red solid (37% yield). ^{1}H NMR (600 MHz, Chloroform-*d*) *δ* 6.66 (s, 1H), 6.27 (s, 1H), 5.19 (s, 1H), 2.41 (s, 3H), 2.30 (s, 3H), 1.55 (s, 6H).

Synthesis of TPA-Py: To a 100 mL round bottom flask was added compound TPA-Br (1.0567 g, 3.0 mmol), pyridine-4-boronic acid pinacol ester (0.9227 g, 4.5 mmol), tetrakis(triphenylphosphine)palladium (0.3460 g, 0.3 mmol) and THF (14 mL) under an atmosphere of N_2. Then, 2.8 mL of 2 M aq. K_2CO_3 was added. The mixed solution was stirred at 70 °C for 48 h. After the reaction was completed, the mixture was concentrated under reduced pressure. Then the mixture was suspended in ethyl acetate and washed with H_2O. The organic layer was collected, dried over Na_2SO_4, filtered, and concentrated. The crude product was purified by silica gel column chromatography using petroleum ether as an eluent. Finally, reduced pressure afforded the target compound TPA-Py as an orange-yellow oily liquid

(73% yield). ^{1}H NMR (600 MHz, DMSO-d_6) δ 9.81 (s, 1H), 8.62 (d, *J* = 5.7 Hz, 2H), 7.85 (d, *J* = 8.5 Hz, 2H), 7.78 (d, *J* = 8.6 Hz, 2H), 7.71 (d, *J* = 5.8 Hz, 2H), 7.45 (t, *J* = 7.8 Hz, 2H), 7.27 (t, *J* = 6.8 Hz, 3H), 7.23 (d, *J* = 7.7 Hz, 2H), 7.02 (d, *J* = 8.6 Hz, 2H).

A general synthetic procedure for compound MPTCF-2Py and MPTCF-4Py: MPTCF (1 mmol), compound TPA-Py (2.5 mmol) or 4-(bis(4-(pyridin-4-yl)phenyl)amino)benzaldehyde (TPA-2Py, 2.5 mmol) and piperidine (0.2 mL) were dissolved in EtOH/CH_2Cl_2 mixed solution (*v*:*v*, 5:1, 12.0 mL). The reaction mixture was stirred at 50 °C for 12 h under an atmosphere of N_2. After the reaction was completed, the mixture was concentrated under reduced pressure. The crude product was purified by silica gel column chromatography using CH_2Cl_2/MeOH (*v*:*v*, 20:1) as an eluent. Finally, recrystallization using ethyl acetate/hexane afforded the target compounds.

MPTCF-2Py: Dark blue solid (40% yield). ^{1}H NMR (600 MHz, DMSO-d_6) δ 8.61 (d, *J* = 5.7 Hz, 4H), 7.81 (d, *J* = 8.6 Hz, 4H), 7.77 (d, *J* = 12.5 Hz, 2H), 7.75 (d, *J* = 5.3 Hz, 4H), 7.70 (d, *J* = 5.7 Hz, 4H), 7.42 (t, *J* = 7.8 Hz, 4H), 7.21 (t, *J* = 7.4 Hz, 2H), 7.18 (d, *J* = 8.4 Hz, 8H), 7.12 (d, *J* = 16.0 Hz, 2H), 7.08 (d, *J* = 8.6 Hz, 4H), 6.95 (s, 2H), 5.89 (s, 1H), 1.60 (s, 6H).

MPTCF-4Py: Dark blue solid (44% yield). ^{1}H NMR (600 MHz, DMSO-d_6) δ 8.62 (d, *J* = 5.0 Hz, 8H), 7.85 (d, *J* = 8.2 Hz, 8H), 7.80-7.77 (m, 6H), 7.72 (d, *J* = 5.0 Hz, 8H), 7.25 (d, *J* = 8.3 Hz, 8H), 7.18−7.14 (m, 6H), 6.96 (s, 2H), 5.90 (s, 1H), 1.61 (s, 6H).

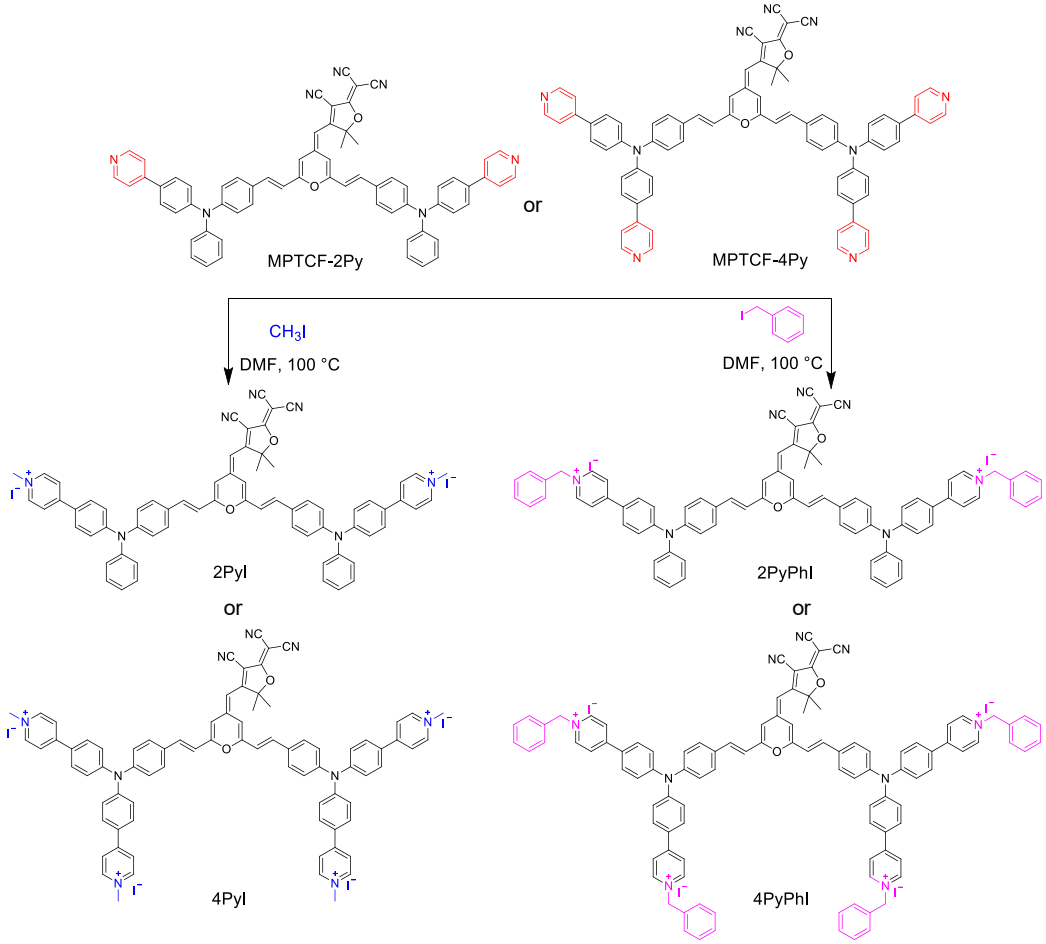

Scheme S2. Synthetic routes to compounds 2PyI, 4PyI, 2PyPhI and 4PyPhI.

A general synthetic route to compounds 2PyI, 4PyI, 2PyPhI and 4PyPhI: Compound MPTCF-2Py (1.0 mmol) or MPTCF-4Py (1.0 mmol) was mixted with methyl iodide (30 mmol) or benzyl iodide (30 mmol) in DMF (3.0 mL). The resulting suspension was stirred at 100 °C for 24 h under an atmosphere of N_2. After the reaction was completed, ethyl acetate was added under ultrasonication, and black precipitates were observed. The crude solid was filtered and successively washed with excess ethyl acetate, tolunene and ethyl ether. The solid were further dissolved in a small amount of DMF and ethyl acetate was added under ultrasonication. The black solid was again filtered and successively washed with excess ethyl acetate, tolunene and ethyl ether. Pure compounds were obtained by repeating the above procedures several times.

2PyI: dark green solid (87% yield). ^{1}H NMR (600 MHz, DMSO-d_6) δ 8.91 (d, *J* = 6.2 Hz, 4H), 8.41 (d, *J* = 6.3 Hz, 4H), 8.06 (d, *J* = 8.6 Hz, 4H), 7.82 (d, *J* = 8.3 Hz, 4H), 7.78 (d, *J* = 16.2 Hz, 2H), 7.47 (t, *J* = 7.7 Hz, 4H), 7.29 (t, *J* = 7.3 Hz, 2H), 7.22 (d, *J* = 7.8 Hz, 4H), 7.18−7.14 (m, 10H), 6.98 (s, 2H), 5.93 (s, 1H), 4.29 (s, 6H), 1.61 (s, 6H). ^{13}C NMR (151 MHz, DMSO) δ 179.28, 173.11, 159.16, 153.61, 150.72, 150.60, 148.00, 145.85, 145.66, 136.90, 131.14, 130.66, 130.22, 130.03, 126.89, 126.59, 126.22, 124.58, 123.08, 122.39, 118.86, 114.85, 114.05, 113.61, 101.63, 97.91, 86.16, 54.93, 48.40, 47.23, 26.34.HRMS (MALDI-TOF): m/z: $[M-I]^+$ calcd for $C_{68}H_{53}N_7O_2^{2+}$: 499.7125; found: 499.7134, m/z: $[I]^+$ calcd for I^-: 126.9050; found: 126.9049.

4PyI: dark green solid (88% yield). ^{1}H NMR (600 MHz, DMSO-d_6) δ 8.95 (d, *J* = 6.6 Hz, 8H), 8.46 (d, *J* = 6.6 Hz, 8H), 8.13 (d, *J* = 8.7 Hz, 8H), 7.89 (d, *J* = 8.4 Hz, 4H), 7.82 (d, *J* = 16.0 Hz, 2H), 7.32 (d, *J* = 8.6 Hz, 8H), 7.29 (d, *J* = 8.4 Hz, 4H), 7.25 (d, *J* = 16.0 Hz, 2H), 7.00 (s, 2H), 5.96 (s, 1H), 4.31 (s, 12H), 1.62 (s, 6H). ^{13}C NMR (151 MHz, DMSO) δ 179.29, 173.45, 158.93, 153.52, 149.75, 147.23, 145.84, 136.58, 132.49, 130.28, 128.58, 126.11, 124.65, 123.59, 119.70, 114.77, 113.99, 113.49, 101.81, 98.05, 86.74, 54.92, 47.41, 26.31. HRMS (MALDI-TOF): m/z: $[M-I]^+$ calcd for $C_{80}H_{65}N_9O_2^{4+}$: 295.8810; found: 295.8818, m/z: $[I]^+$ calcd for I^-: 126.9050; found: 126.9049.

2PyPhI: dark green solid (89% yield). ^{1}H NMR (600 MHz, DMSO-d_6) δ 9.08 (d, *J* = 6.6 Hz, 4H), 8.41 (d, *J* = 6.6 Hz, 4H), 8.03 (d, *J* = 8.6 Hz, 4H), 7.80 (d, *J* = 8.4 Hz, 4H), 7.77 (d, *J* = 16.3 Hz, 2H), 7.54 (d, *J* = 7.4 Hz, 4H), 7.48-7.43 (m, 10H), 7.29 (t, *J* = 7.4 Hz, 2H), 7.22 (d, *J* = 7.8 Hz, 4H), 7.18 (d, *J* = 8.2 Hz, 4H), 7.16 (d, *J* = 14.0 Hz, 2H), 7.13 (d, *J* = 8.6 Hz, 4H), 6.97 (s, 2H), 5.91 (s, 1H), 5.77 (s, 4H), 1.61 (s, 6H). ^{13}C NMR (151 MHz, DMSO) δ 179.28, 173.15, 159.12, 154.43, 150.90, 150.53, 147.89, 145.77, 144.82, 136.87, 135.07, 131.28, 130.67, 130.25, 130.21, 129.73, 129.71, 129.10, 126.95, 126.38, 126.30, 124.76, 123.80, 122.13, 118.95, 114.84, 114.03, 113.58, 101.64, 97.92, 86.24, 62.57, 48.46, 26.33, 21.54. HRMS (MALDI-TOF): m/z: $[M-I]^+$ calcd for $C_{80}H_{61}N_7O_2^{2+}$: 575.7438; found: 575.7451, m/z: $[I]^+$ calcd for I^-: 126.9050; found: 126.9047.

4PyPhI: dark green solid (88% yield). ^{1}H NMR (600 MHz, DMSO-d_6) δ 9.14 (d, *J* = 6.5 Hz, 8H), 8.47 (d, *J* = 6.5 Hz, 8H), 8.10 (d, *J* = 8.5 Hz, 8H), 7.87 (d, *J* = 8.2 Hz, 4H), 7.80 (d, *J* = 16.2 Hz, 2H), 7.55 (d, *J* = 7.1 Hz, 8H), 7.48−7.43 (m, 12H), 7.30 (d, *J* = 8.5 Hz, 8H), 7.28 (d, *J* = 7.7 Hz, 4H), 7.22 (d, *J* = 16.1 Hz, 2H), 6.99 (s, 2H), 5.94 (s, 1H), 5.82 (s, 8H), 1.62 (s, 6H). ^{13}C NMR

(151 MHz, DMSO) δ 179.28, 173.47, 158.87, 154.38, 150.29, 149.87, 147.11, 145.01, 136.53, 134.99, 132.63, 130.48, 130.42, 129.78, 129.73, 129.14, 128.50, 126.31, 124.57, 124.39, 119.77, 114.73, 113.94, 113.47, 101.82, 98.06, 86.83, 62.76, 48.79, 26.32. HRMS (MALDI-TOF): m/z: $[M-I]^+$ calcd for $C_{104}H_{81}N_9O_2^{4+}$: 371.9123; found: 371.9135, m/z: $[I]^+$ calcd for I^-: 126.9050; found: 126.9049.

Supplementary figures

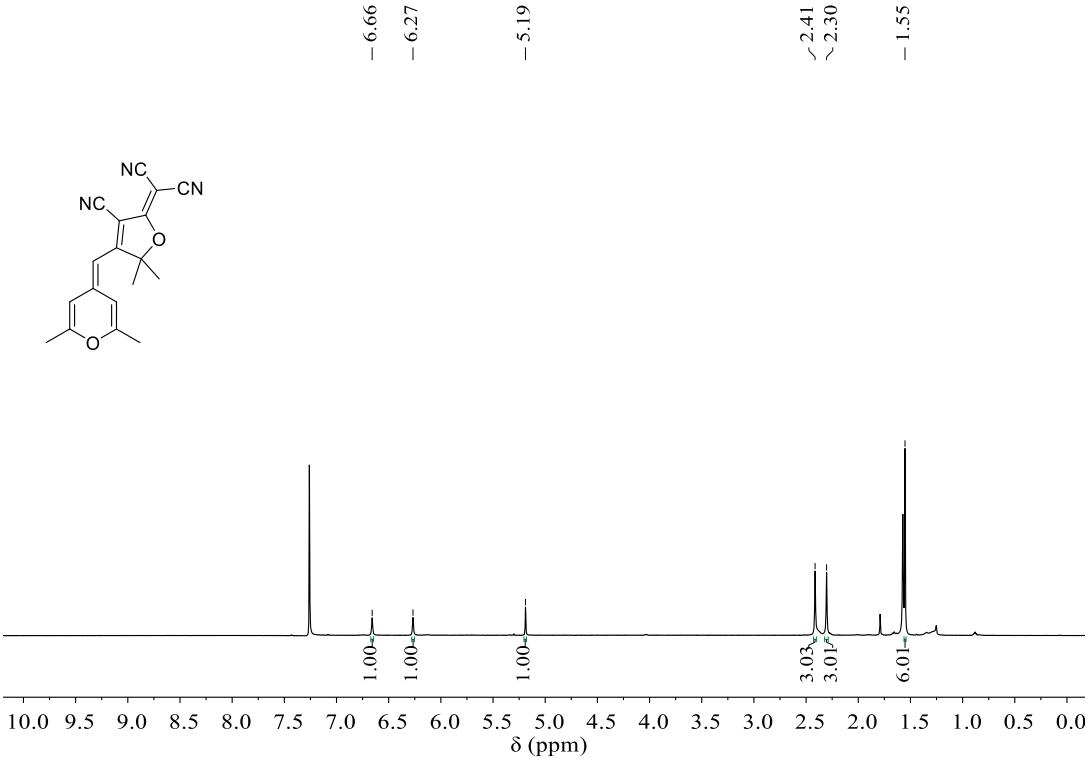

Figure S1. ^{1}H NMR spectrum of MPTCF in $CDCl_3$.

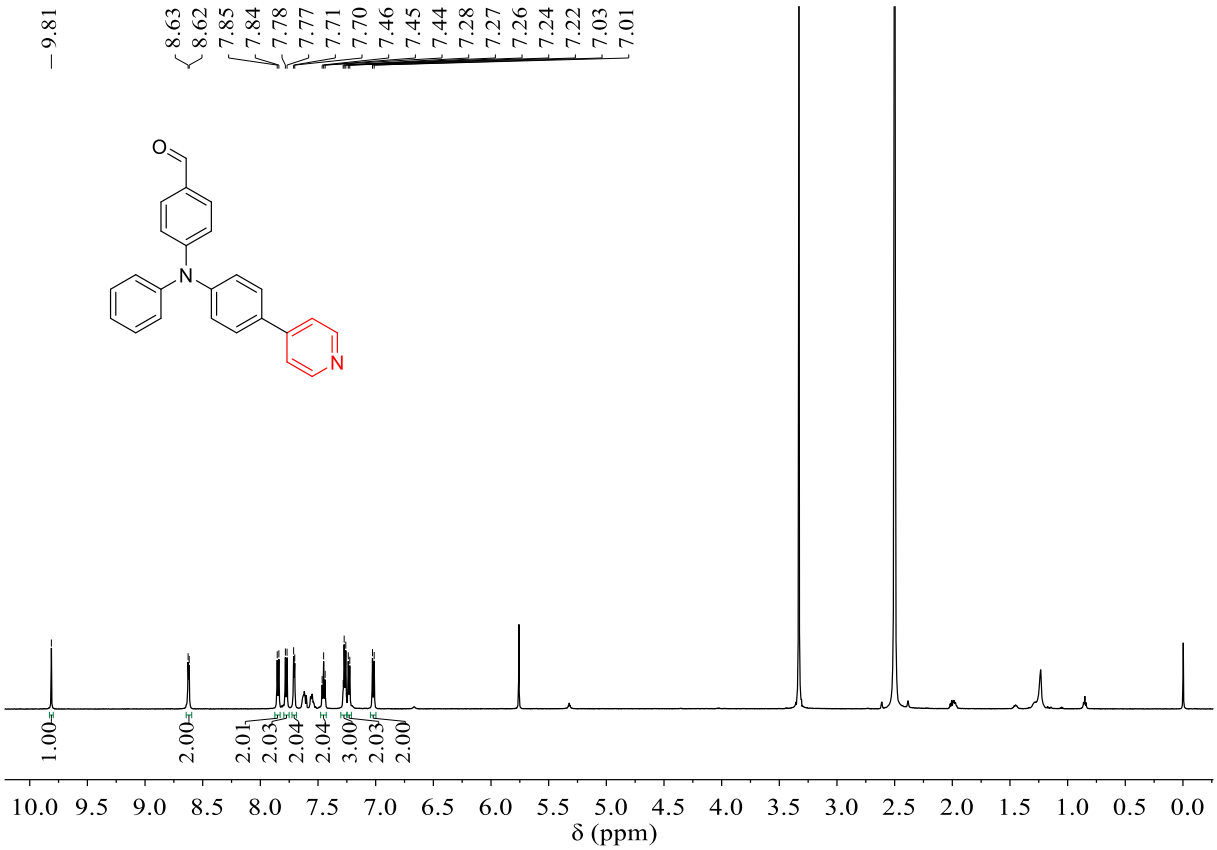

Figure S2. ^{1}H NMR spectrum of TPA-Py in DMSO-d_6.

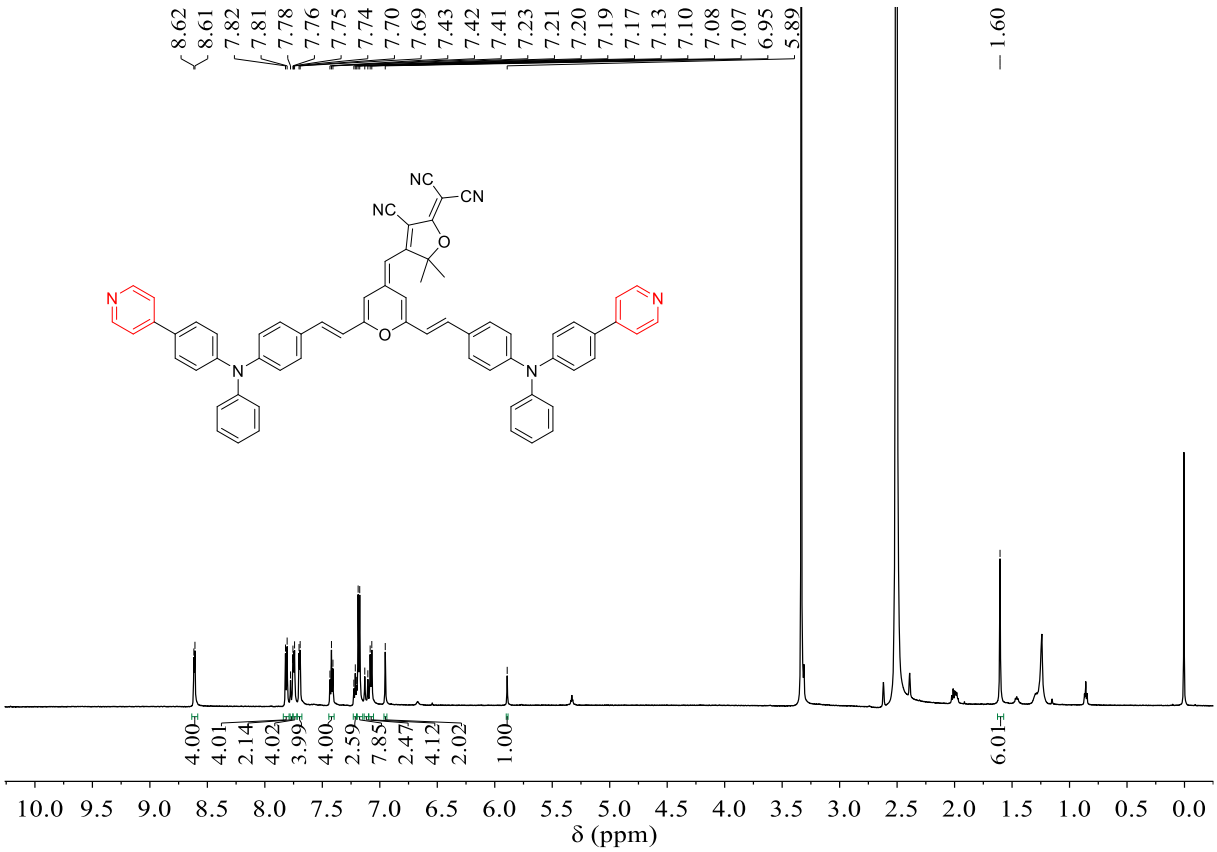

Figure S3. ^{1}H NMR spectrum of MPTCF-2Py in DMSO-d_6.

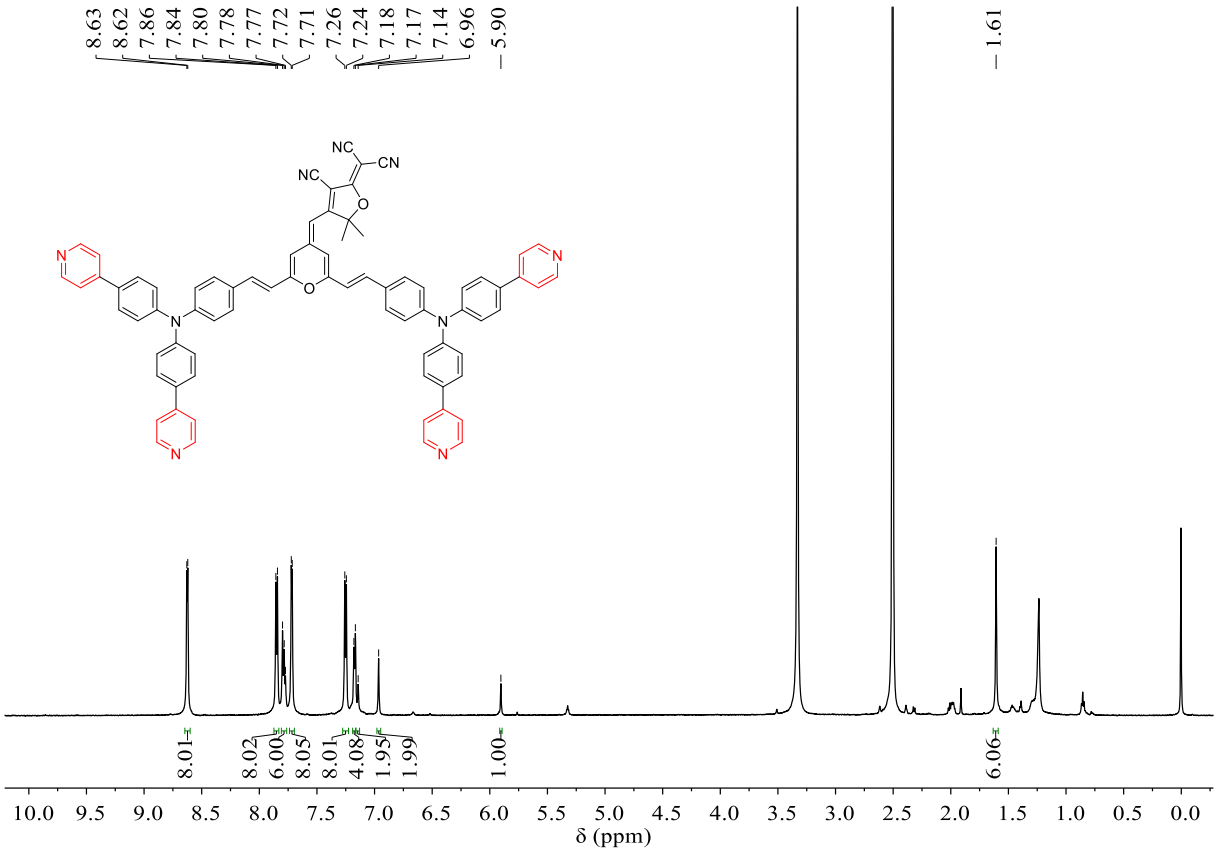

Figure S4. ^{1}H NMR spectrum of MPTCF-4Py in DMSO-d_6.

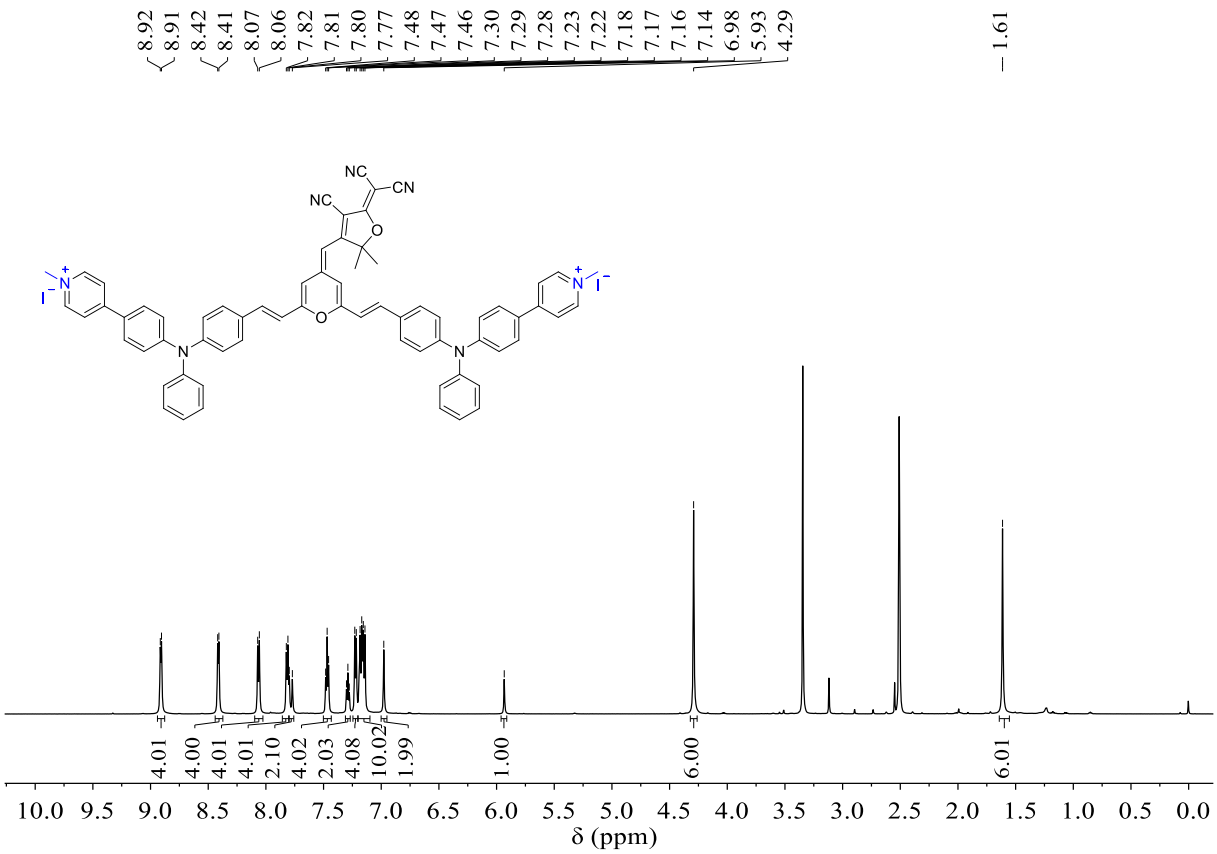

Figure S5. ^{1}H NMR spectrum of 2PyI in DMSO-d_6.

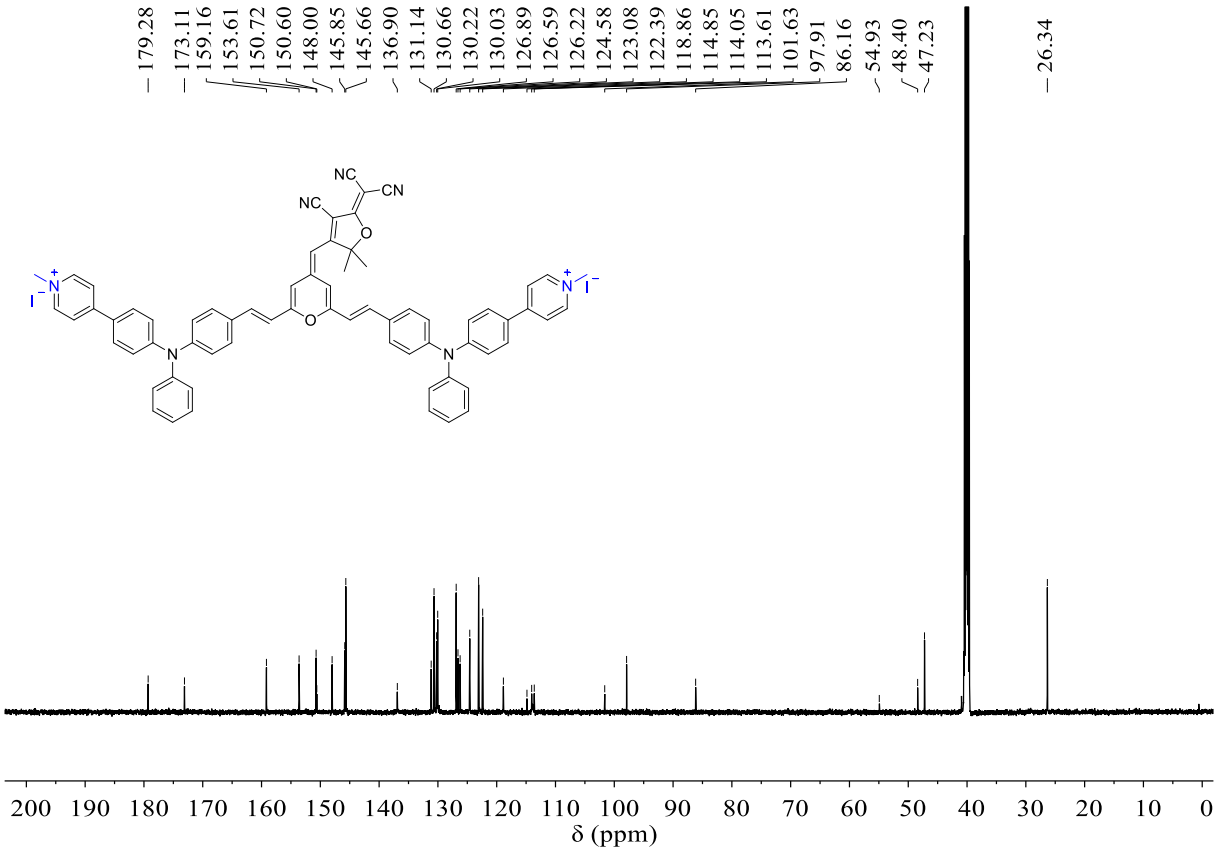

Figure S6. ^{13}C NMR spectrum of 2PyI in DMSO-d_6.

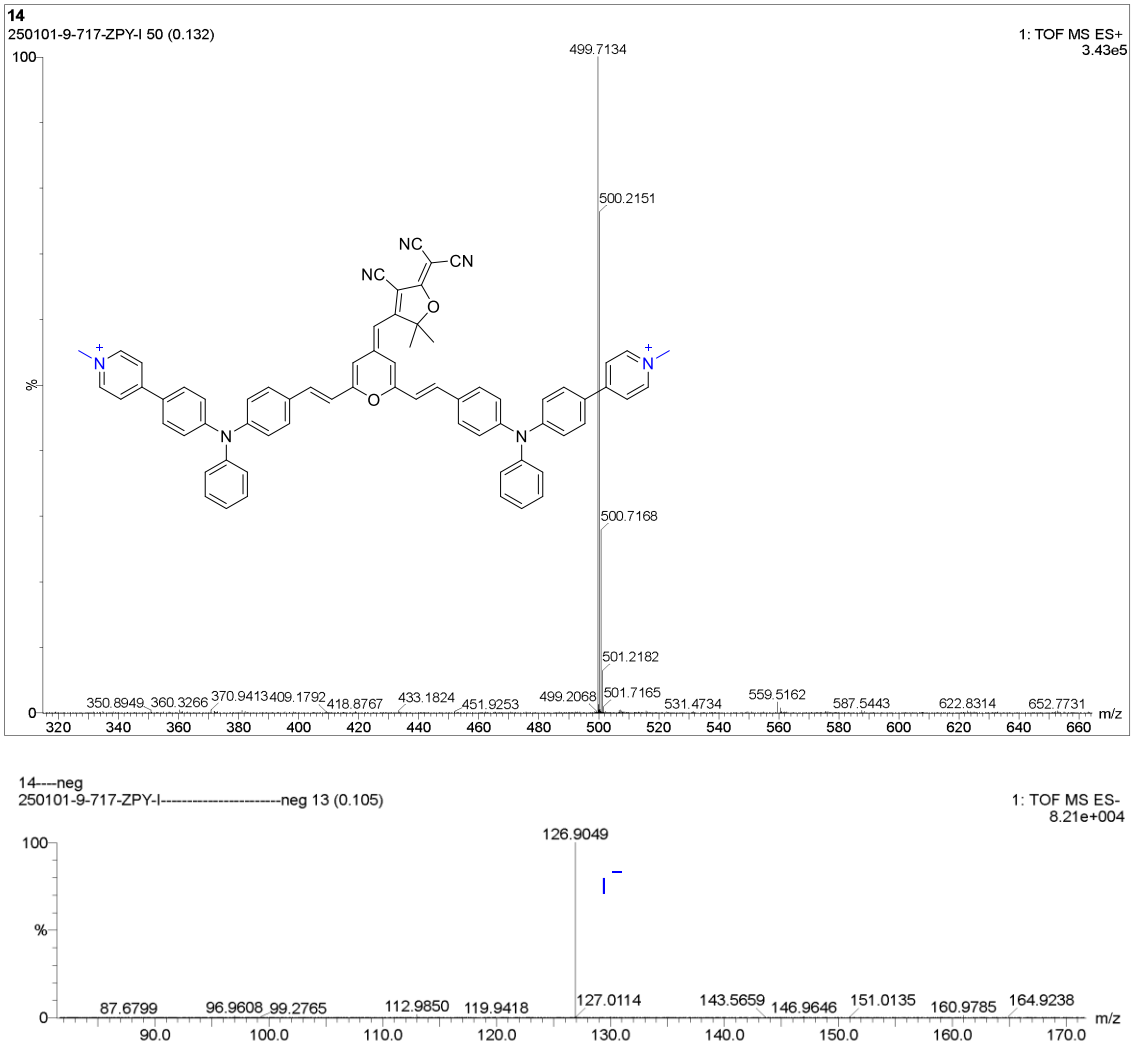

Figure S7. HRMS spectrum of 2PyI.

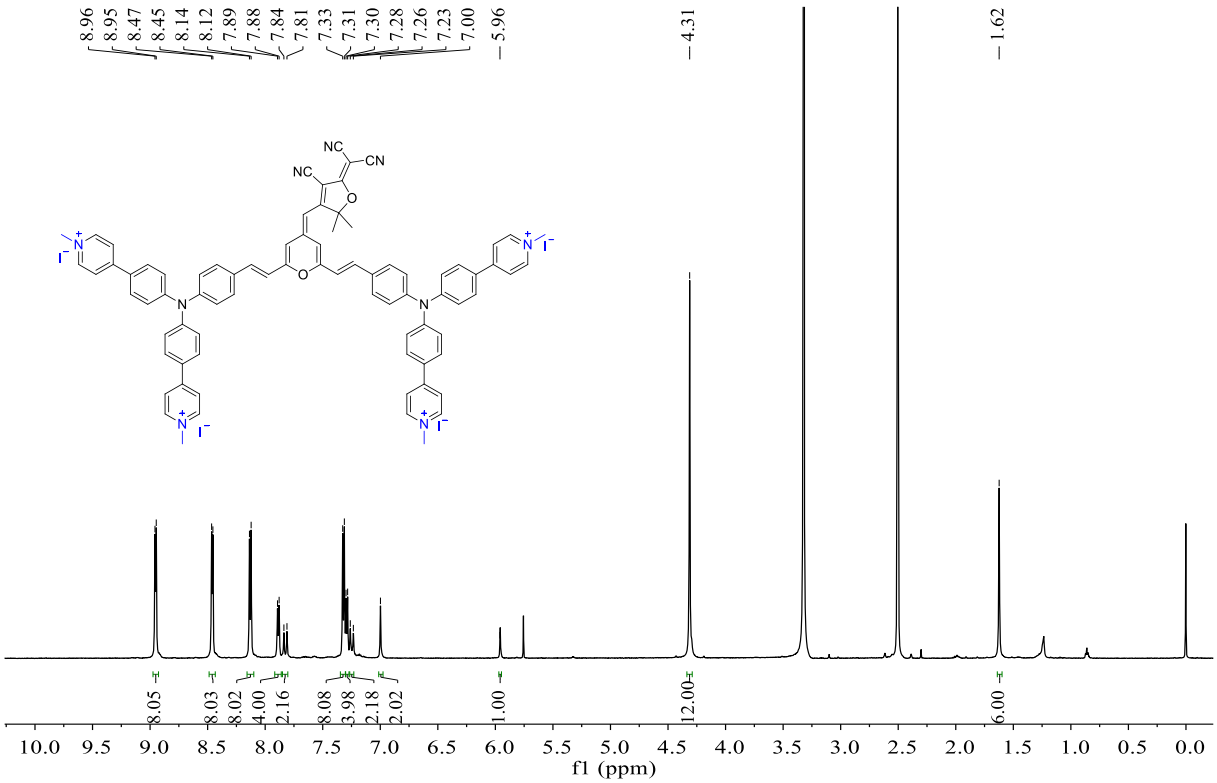

Figure S8. ^{1}H NMR spectrum of 4PyI in DMSO-d_6.

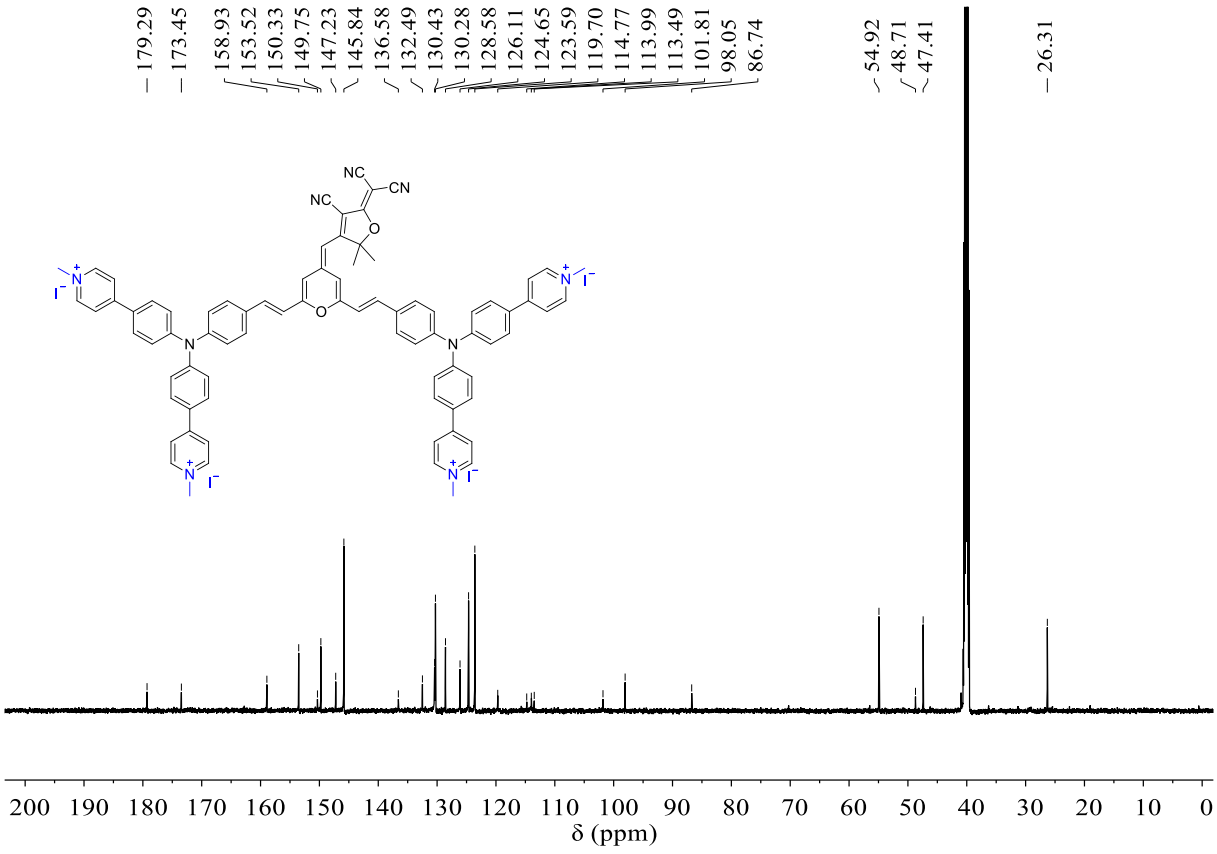

Figure S9. ^{13}C NMR spectrum of 4PyI in DMSO-d_6.

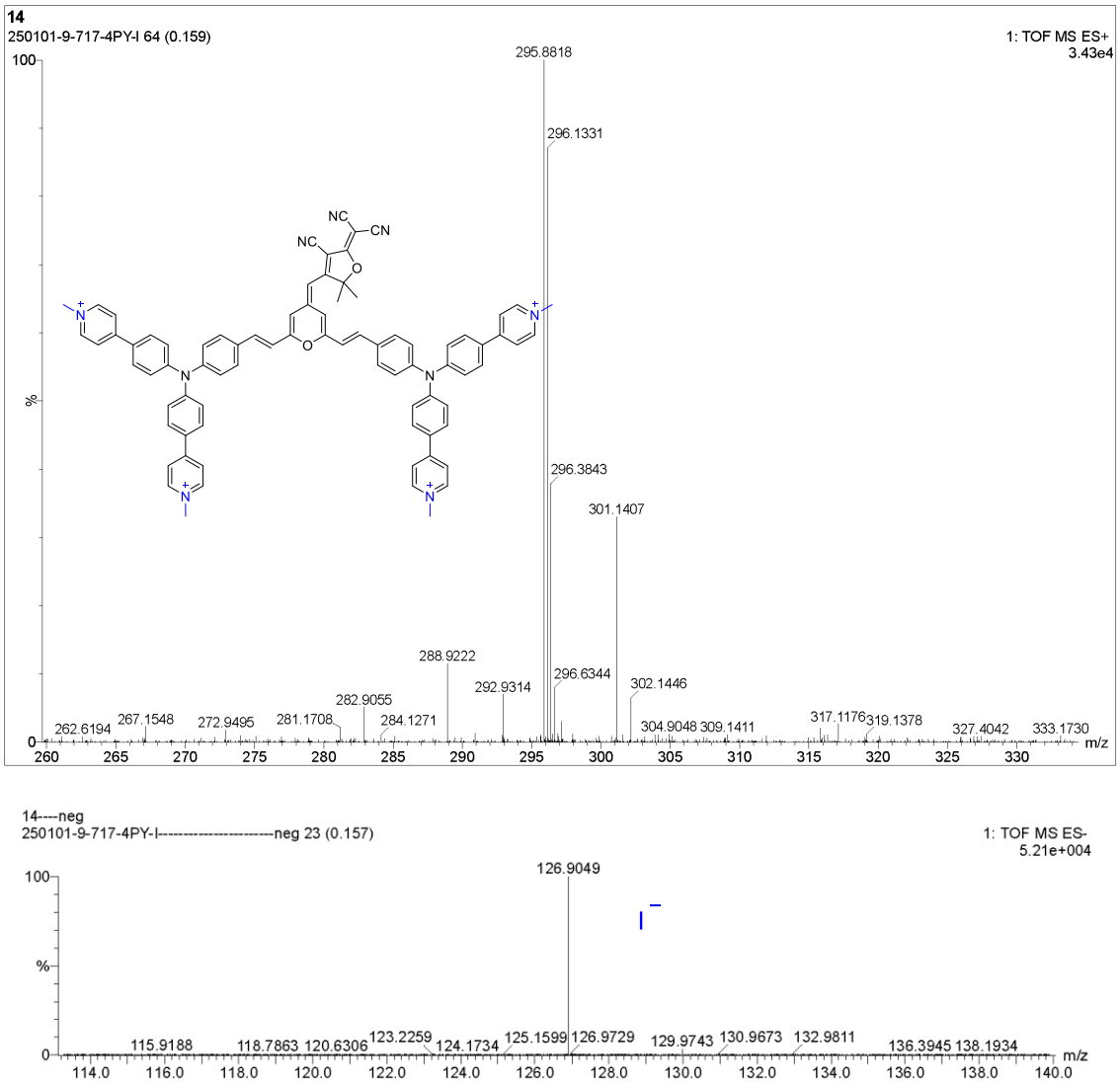

Figure S10. HRMS spectrum of 4PyI.

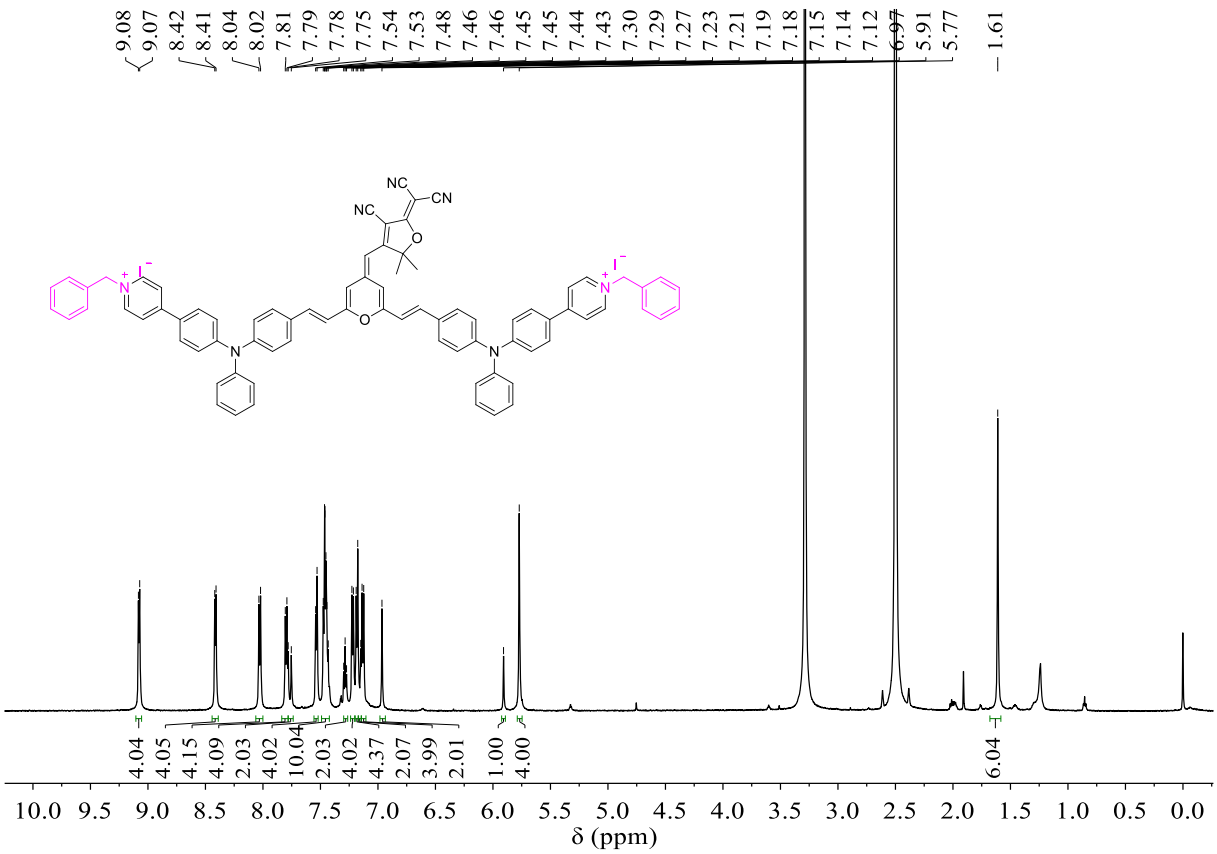

Figure S11. ^{1}H NMR spectrum of 2PyPhI in DMSO-d_6.

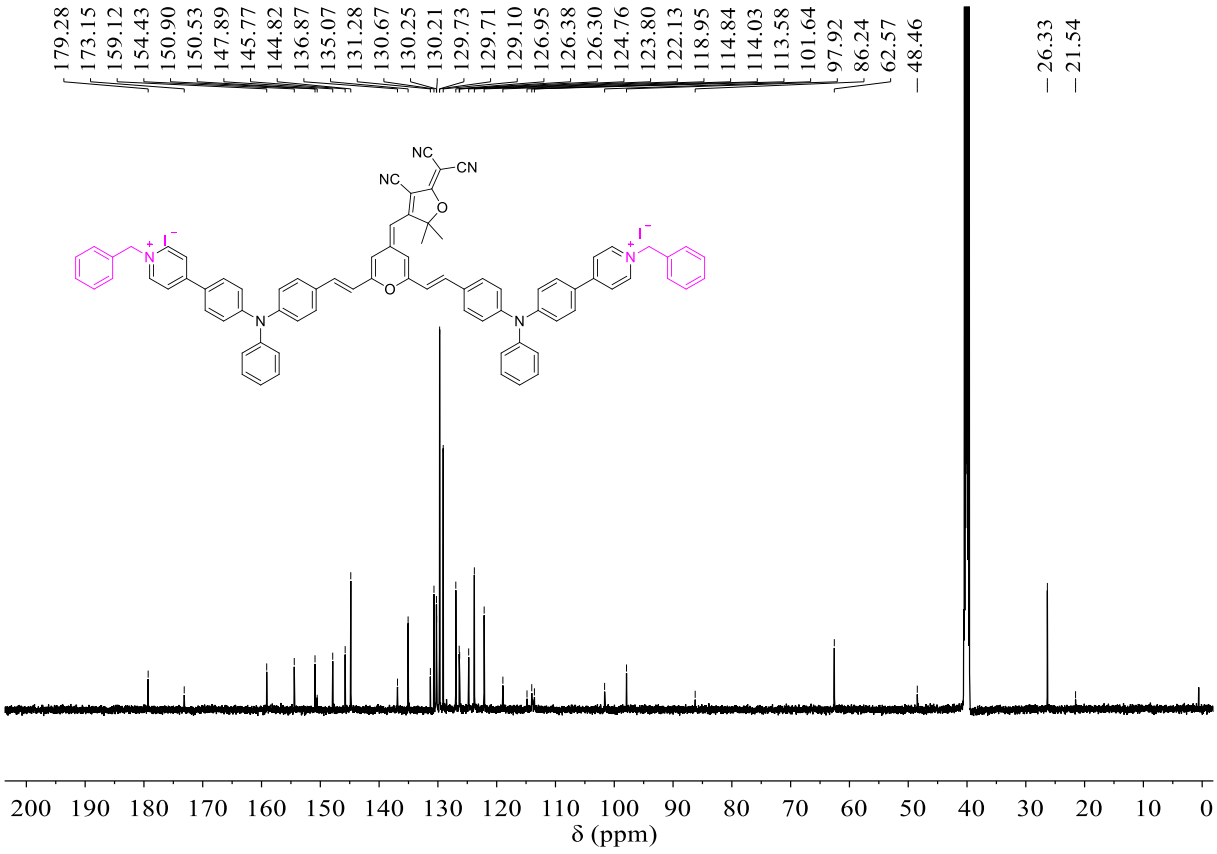

Figure S12. ^{13}C NMR spectrum of 2PyPhI in DMSO-d_6.

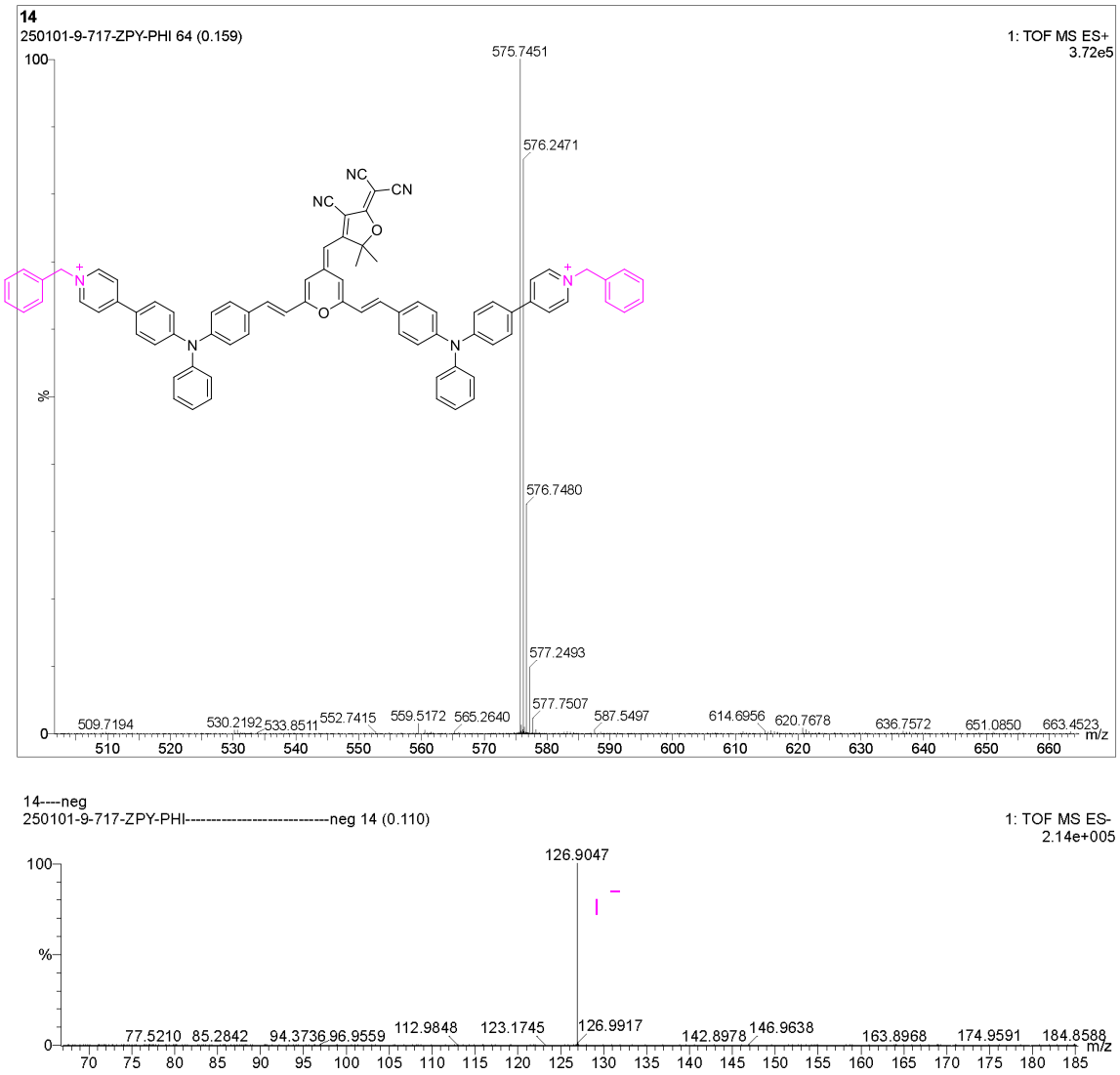

Figure S13. HRMS spectrum of 2PyPhI.

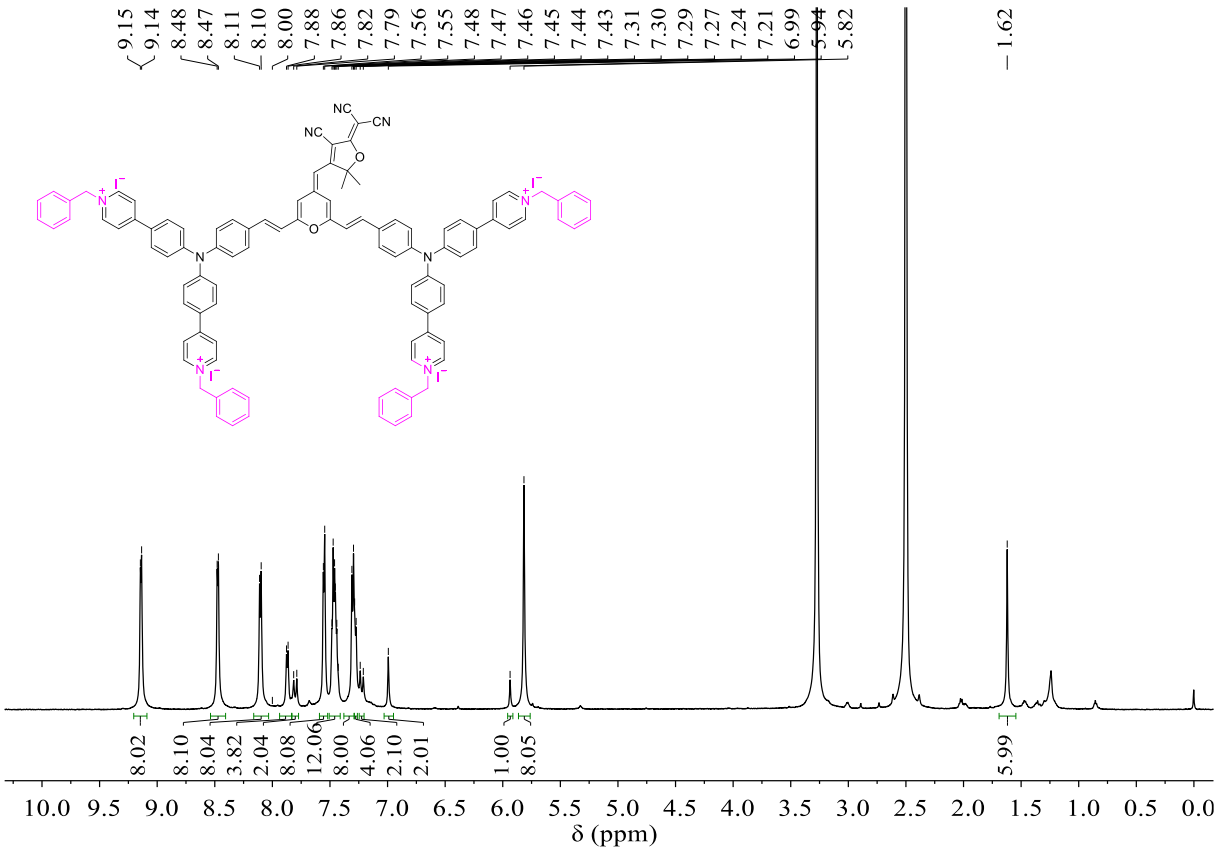

Figure S14. ^{1}H NMR spectrum of 4PyPhI in DMSO-d_6.

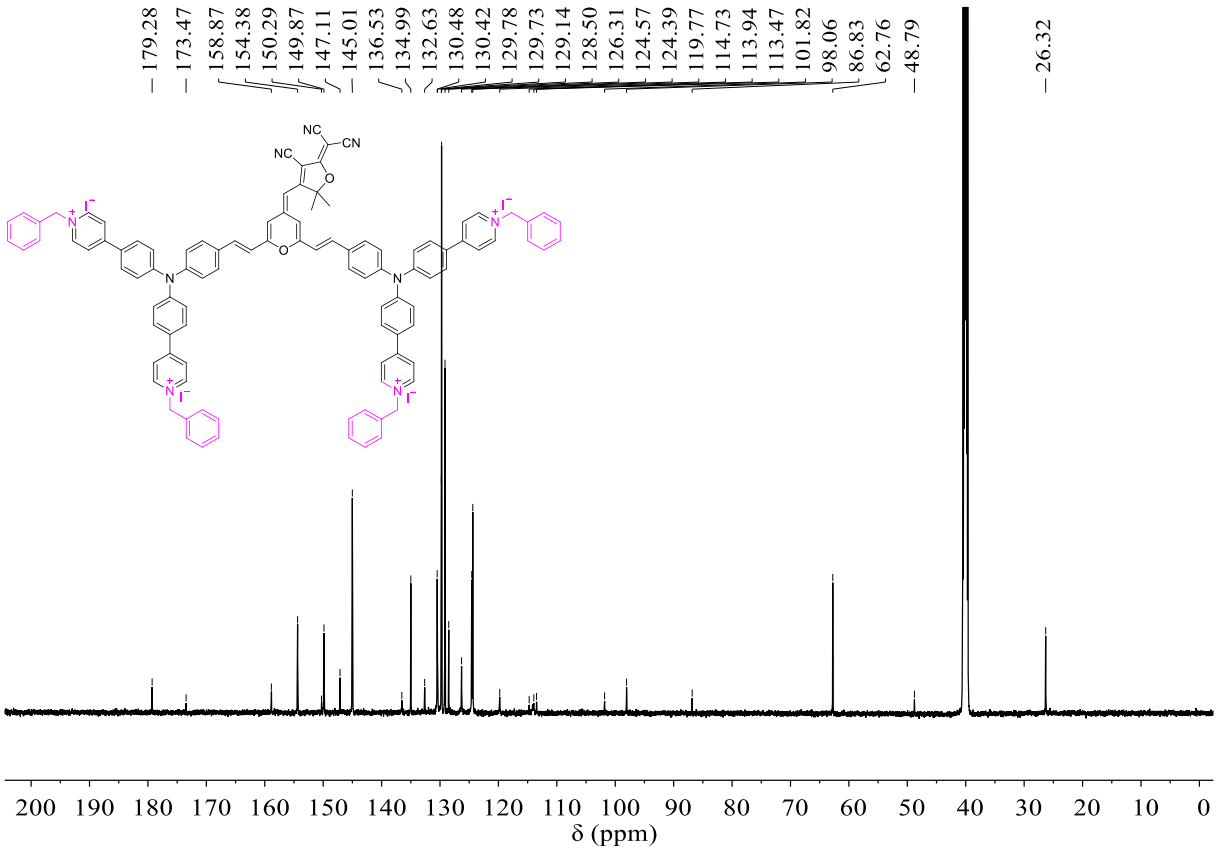

Figure S15. ^{13}C NMR spectrum of 4PyPhI in DMSO-d_6.

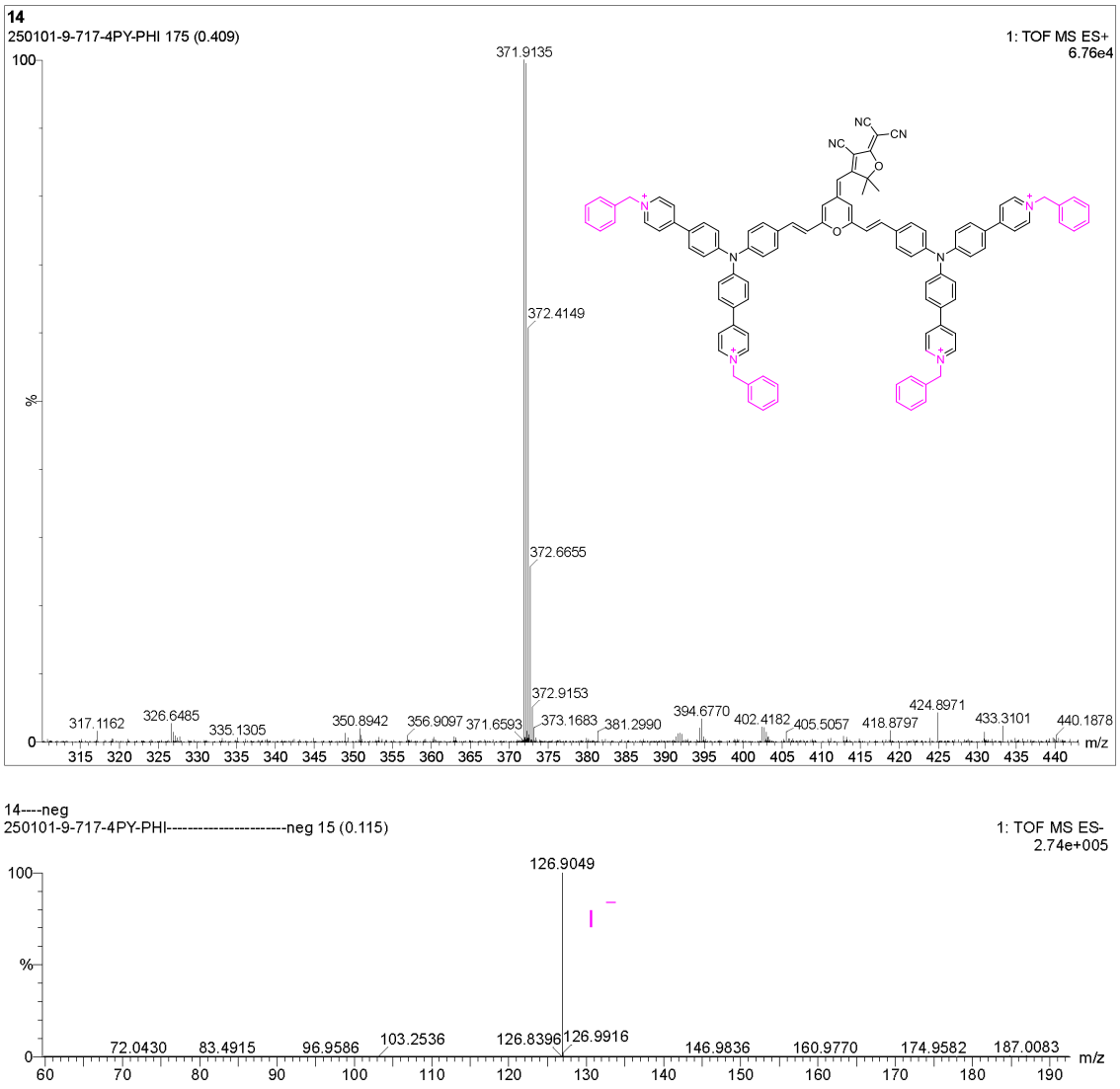

Figure S16. HRMS spectrum of 4PyPhI.

Table S1. Comparison of parameters between the reported ionic OPTAs and 2PyI in this study.

Ref.	Chemical structure	$\lambda_{ex}/\lambda_{em}$ (nm)	PCE	ROS type
4	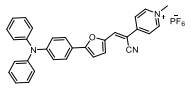	544 (in DMSO)/725 (in toluene)	/	Type I/II
5	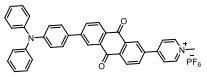	490/540 (in hexane)	/	Type I/II
6	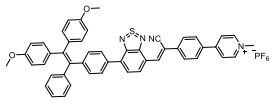	580 (in DMSO)/645 (in toluene)	/	Type I/II
7	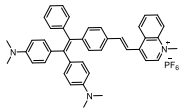	532 (in DMSO)/960 (in water)	/	Type I
8	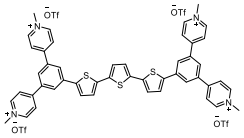	411/~500 nm (in DMSO)	/	Type I/II
9	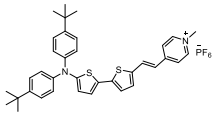	515/802 nm (in THF)	/	Type I
10	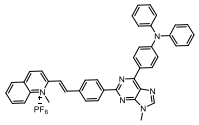	395/725 (in water)	/	Type I/II
11	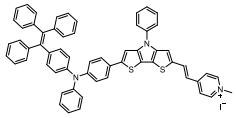	528/735 nm (in DMSO)	/	Type II
12	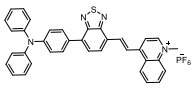	520/760 nm (in DMSO)	60% (532 nm laser)	Type I/II
13	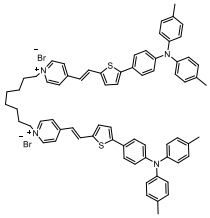	497/675 (in DMSO)	64.19% (520 laser)	Type I/II
14	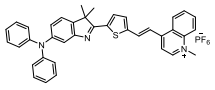	527 (in MeOH)/1048 (in water)	43% (635 nm laser)	Type I/II
This work	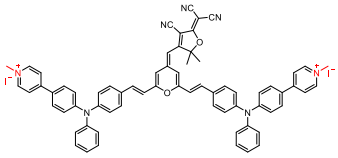	630/955 nm (in DMSO)	42% (660 nm laser)	Type I/II

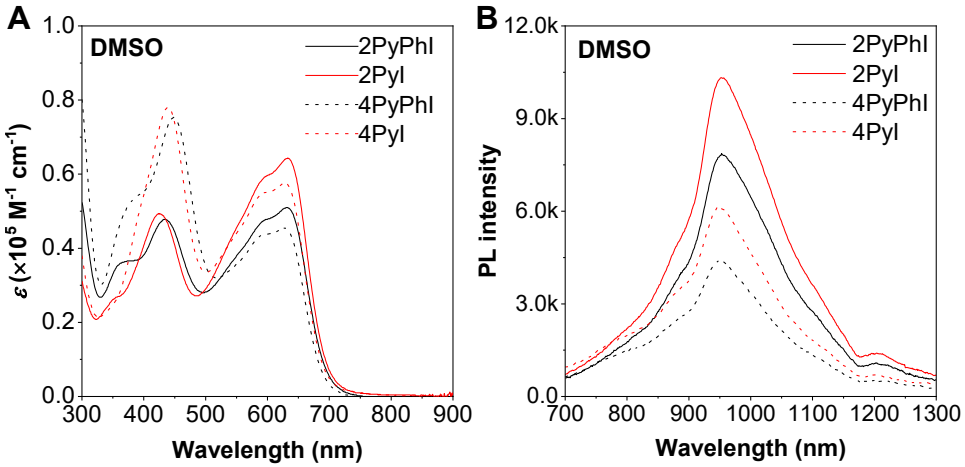

Figure S17. (A) Molar extiction coefficients and (B) photoluminescence (PL) spectra for the four compounds in DMSO solution. E_x = 660 nm.

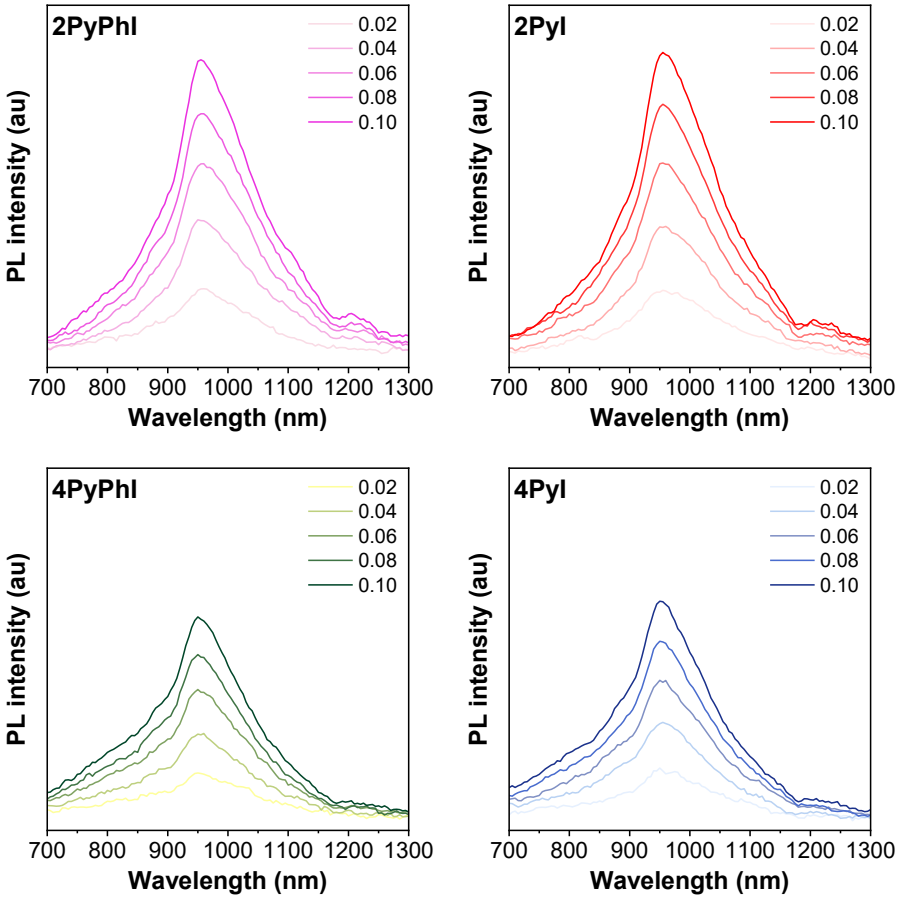

Figure S18. The PL spectra of 2PyPhI, 2Pyl, 4PyPhI and 4Pyl in DMSO at different optical density under 660 nm laser irradiation.

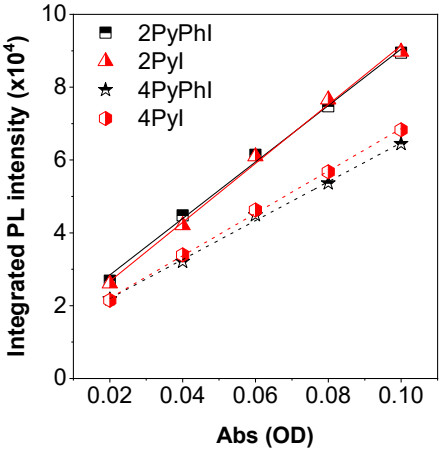

Figure S19. The linear fitting of the integrated PL intensity vs. the absorbance values of different compounds in DMSO solution. E_x=660 nm.

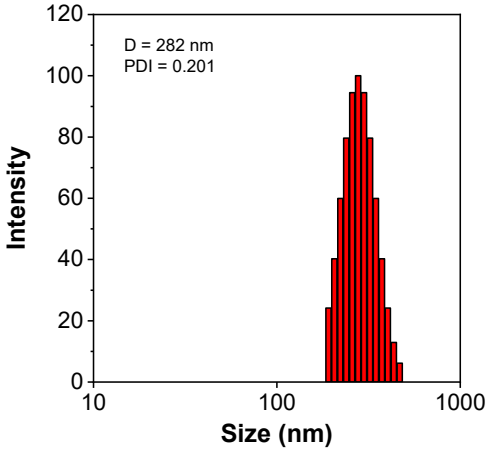

Figure S20. Particle size distribution of 2PyI in aqueous solution. Concentration: 5 μM.

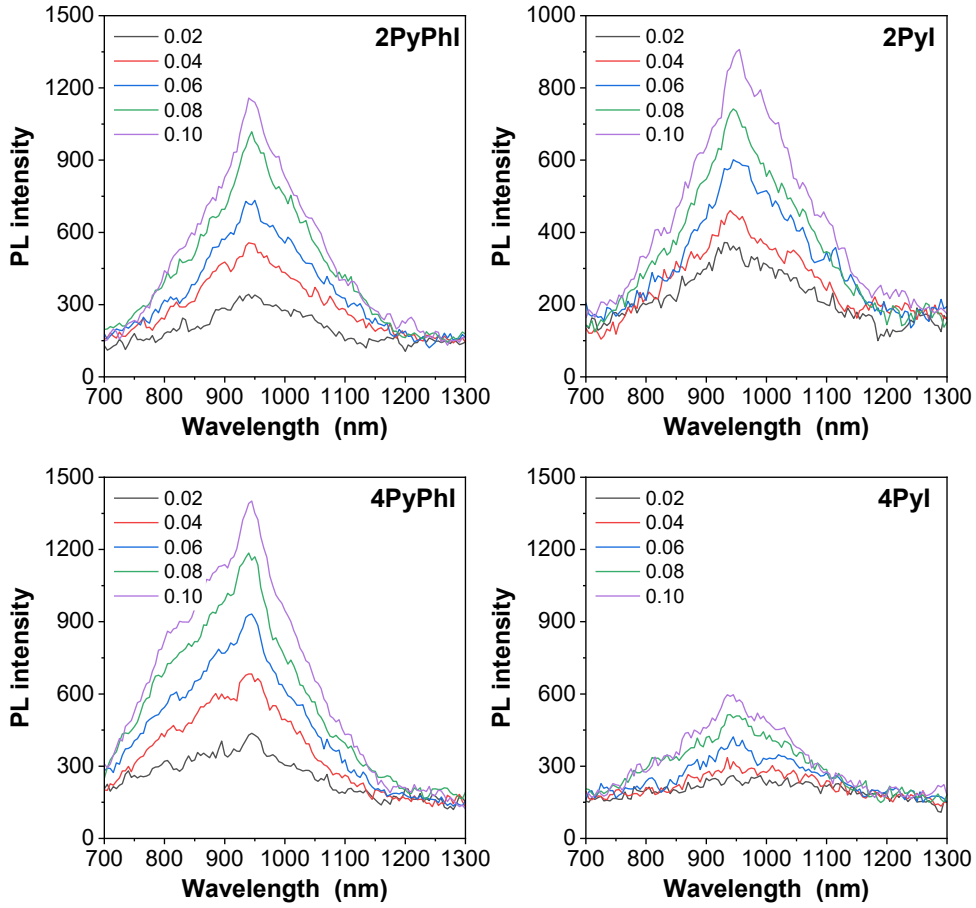

Figure S21. The PL spectra of 2PyPhI, 2PyI, 4PyPhI and 4PyI in aqueous solution at different optical density under 660 nm laser irradiation.

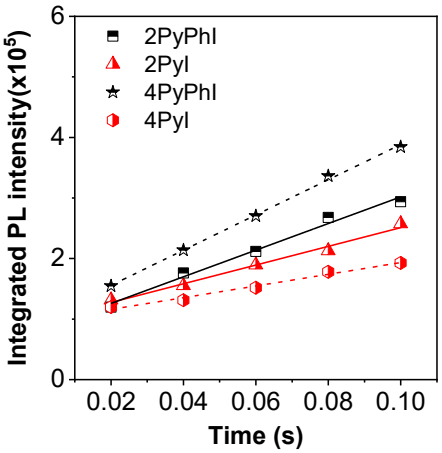

Figure S22. The linear fitting of the integrated PL intensity vs. the absorbance values of different compounds in aqueous solution. E_x=660 nm.

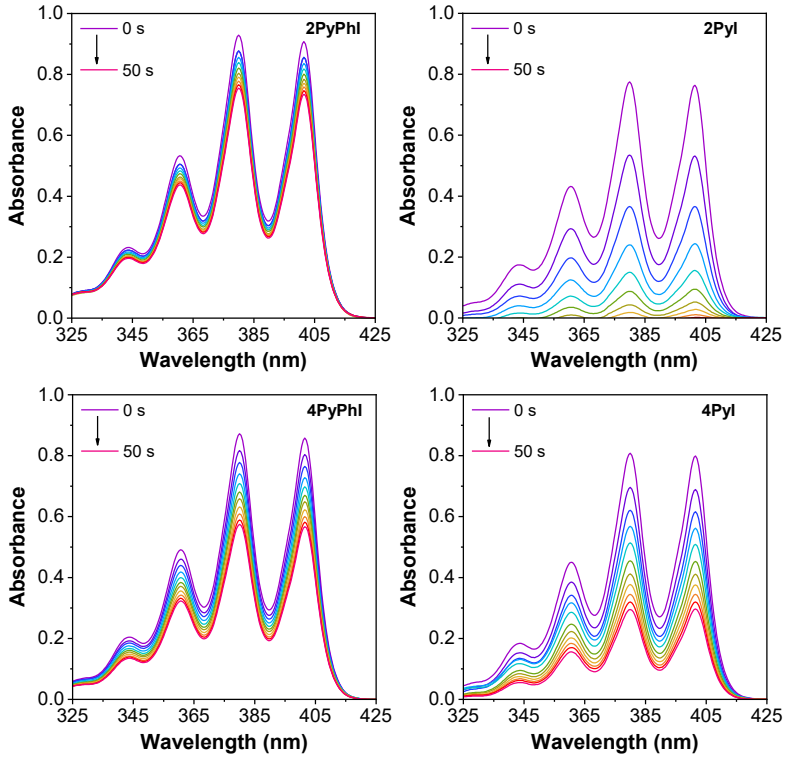

Figure S23. ROS ($^1O_2$) generation capability of the four compounds upon 660 nm laser irradiation (0.1 W cm^{-2}) using ABDA as an indicator. Concentration: 1 μM.

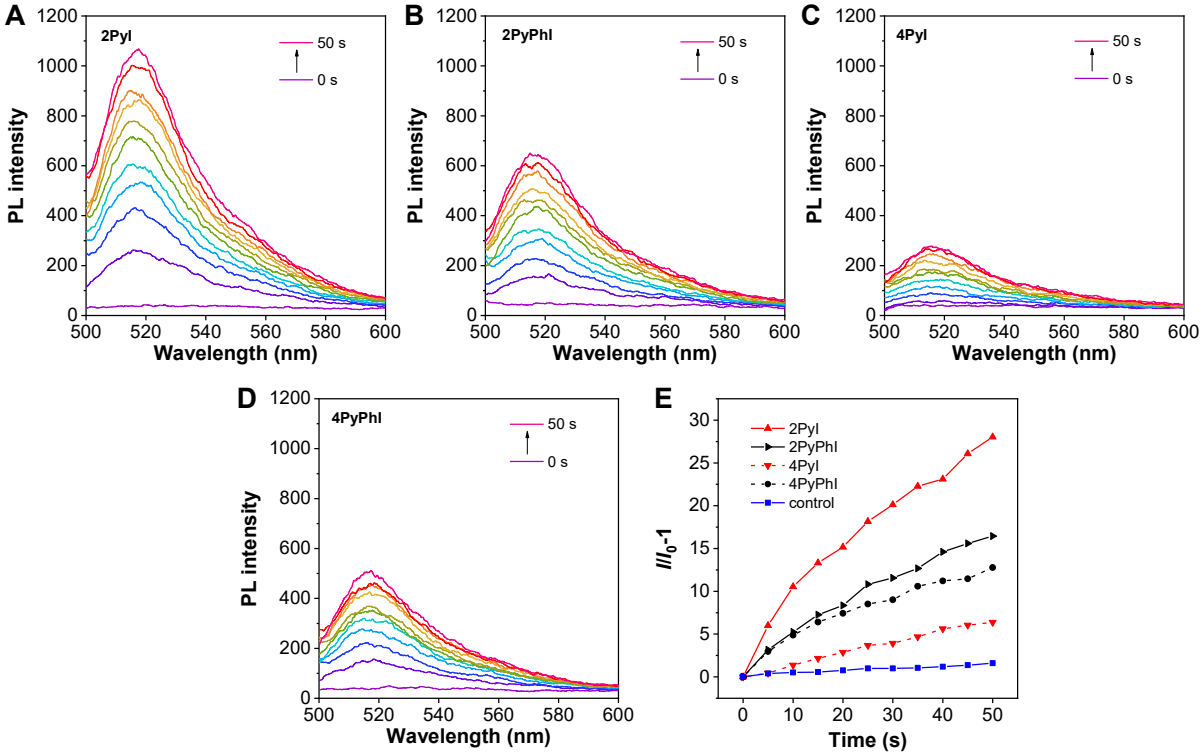

Figure S24. ROS (•OH) generation capability of (A) 2PyI, (B) 2PyPhI, (C) 4PyI and (D) 4PyPhI upon 660 nm laser irradiation (0.1 W cm^{-2}) using APF as an indicator. Concentration: 1 μM. (E) Relative changes in PL intensity of APF in the presence of the four compounds upon 660 nm laser irradiation (0.1 W cm^{-2}) for different times.

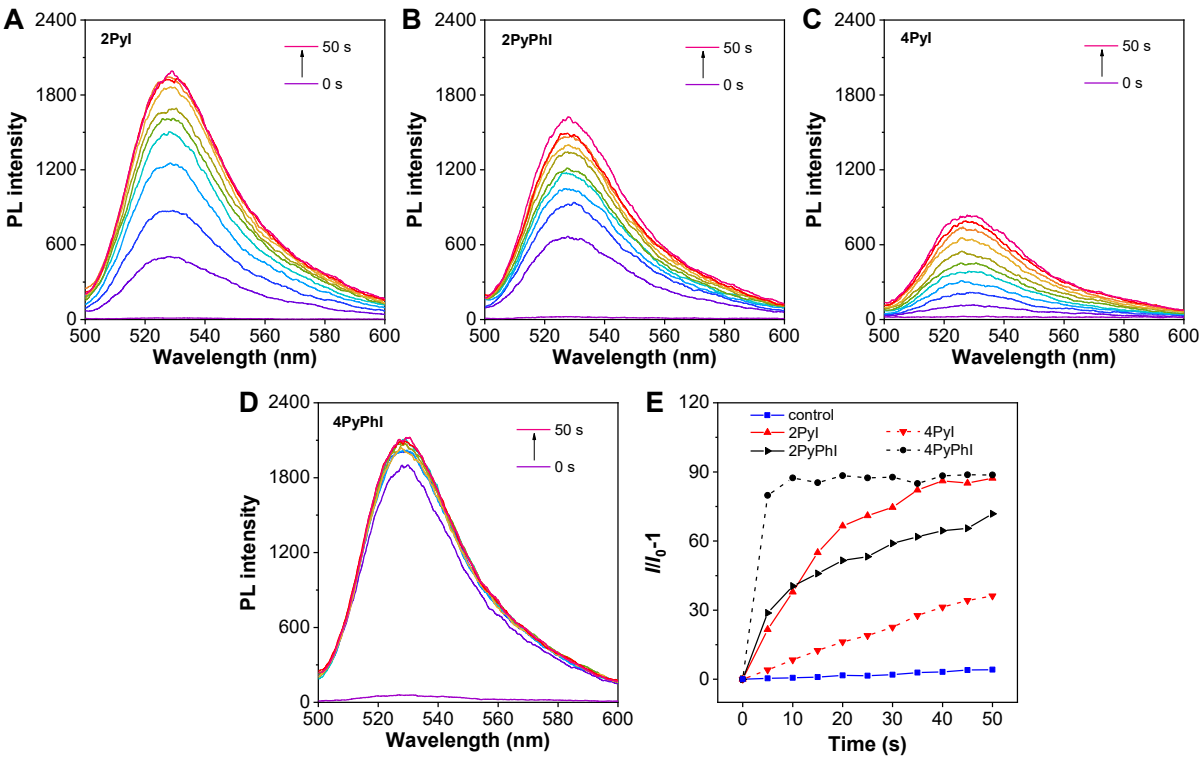

Figure S25. ROS ($O_2^{\bullet-}$) generation capability of (A) 2PyI, (B) 2PyPhI, (C) 4PyI and (D) 4PyPhI upon 660 nm laser irradiation (0.1 W cm^{-2}) using DHR123 as an indicator. Concentration: 1 μM. (E) Relative changes in PL intensity of DHR123 in the presence of the four compounds upon 660 nm laser irradiation (0.1 W cm^{-2}) for different times.

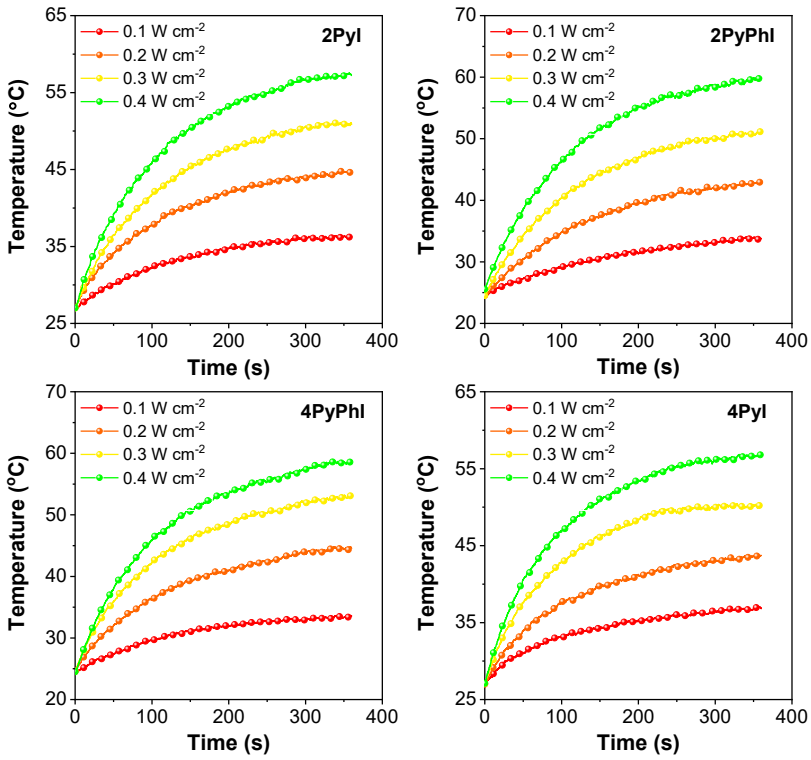

Figure S26. Temperature variation of 2PyI, 2PyPhI, 4PyPhI and 4PyI under 660 nm laser irradiation. (Concentration: 60 μM).

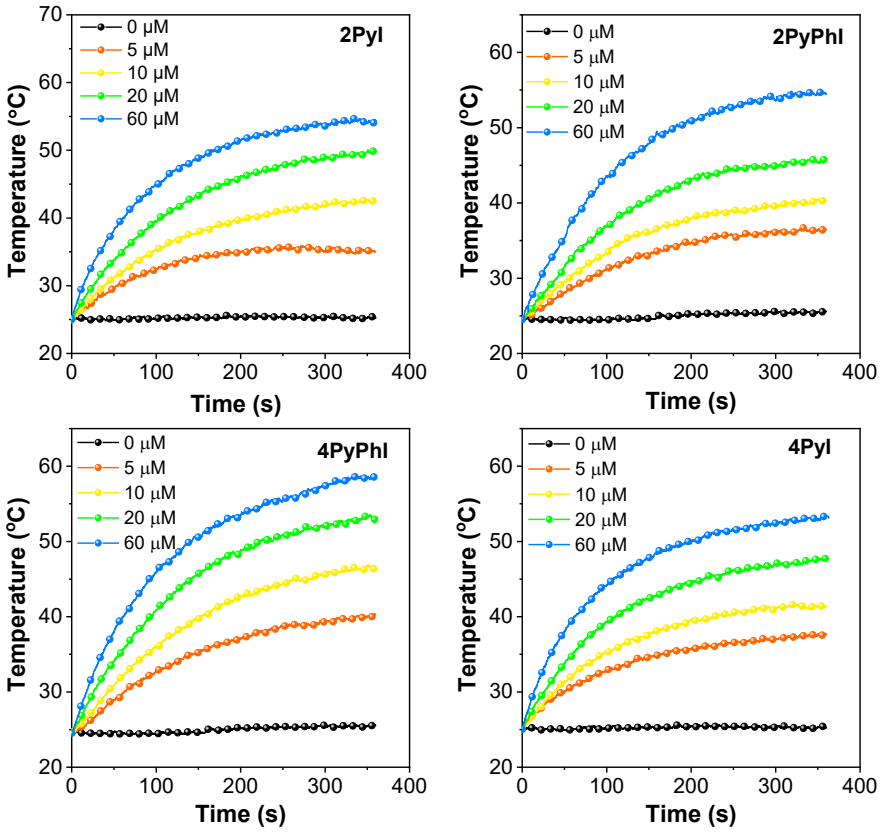

Figure S27. Temperature variations of 2PyI, 2PyPhI, 4PyPhI and 4PyI in aqueous solution at different concentrations under 660 nm laser irradiation (0.4 W cm^{-2}).

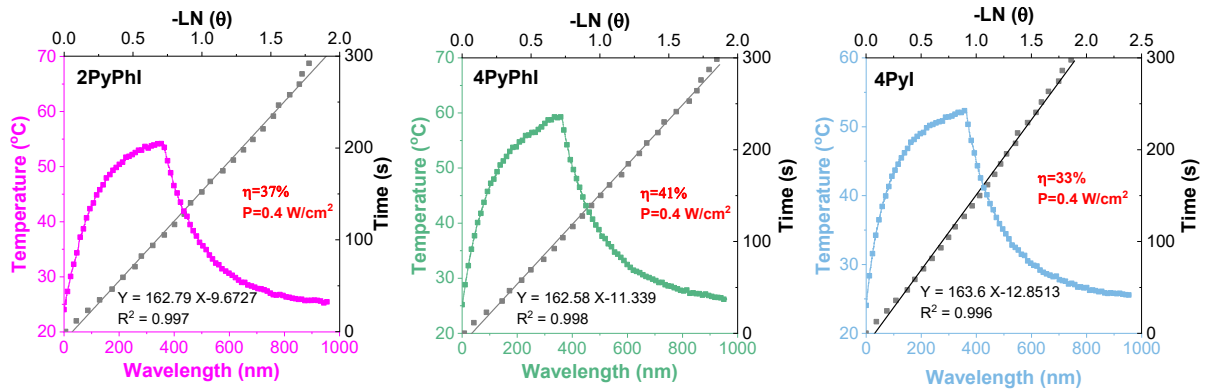

Figure S28. Temperature-increasing/decreasing curve and cooling time *vs*-ln(θ) plot of 2PyPhI, 4PyPhI and 4PyI in aqueous solution upon 660 nm laser irradiation (0.4 W cm^{-2}). Concentration: 60 μM.

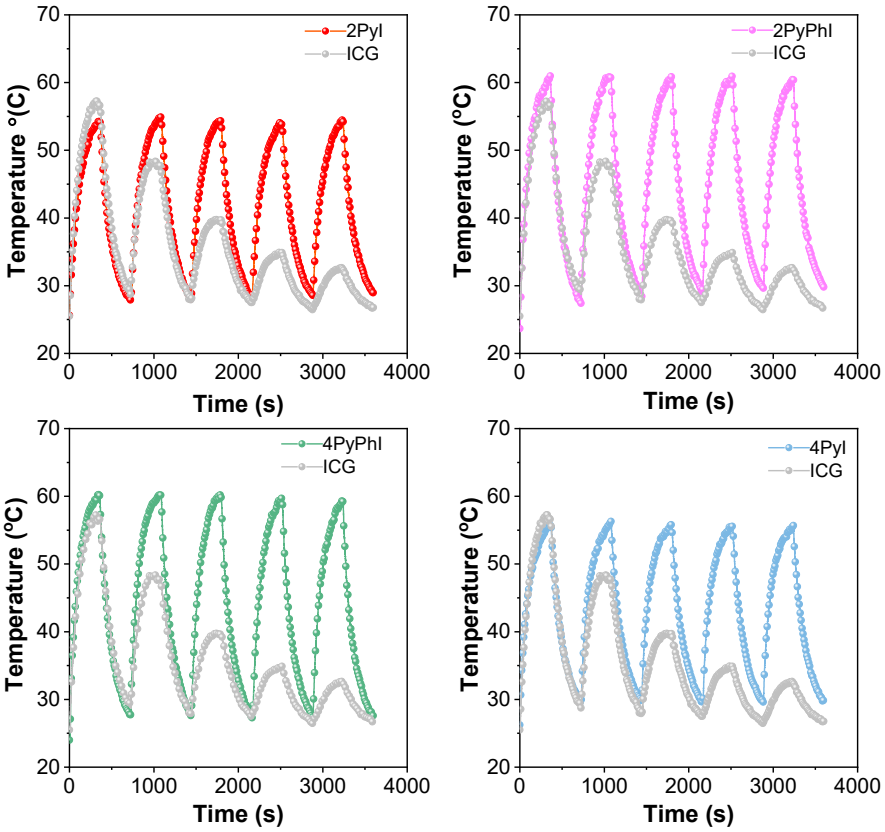

Figure S29. Photothermal stability of 2PyI, 2PyPhI, 4PyPhI and 4PyI in comparison to ICG during 5 cycles of heating-cooling upon 660 nm laser irradiation (0.4 W cm^{-2}). Concentration: 60 μM.

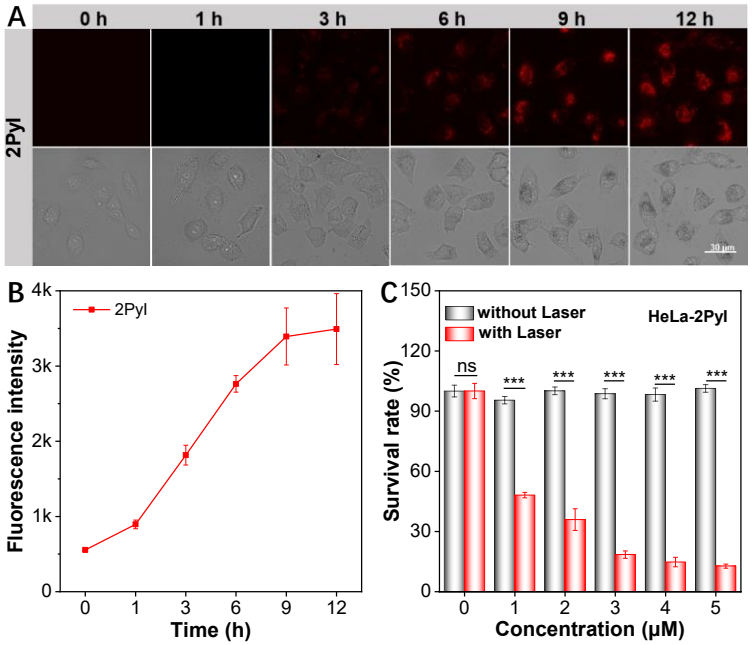

Figure S30. (A) Time-dependent fluorescence images (top) of 2PyI by HeLa cells and the corresponding bright-field images (down). The scale bar represents 30 μm. (B) The corresponding fluorescence intensity vs. different incubation time obtained in (A). (C) In vitro cytotoxicity of 2PyI toward HeLa cells in the absence or presence of 660 nm laser irradiation (0.4 W cm^{-2}). Data were presented as mean ± SD (n = 3, $^{***}p<0.001$).

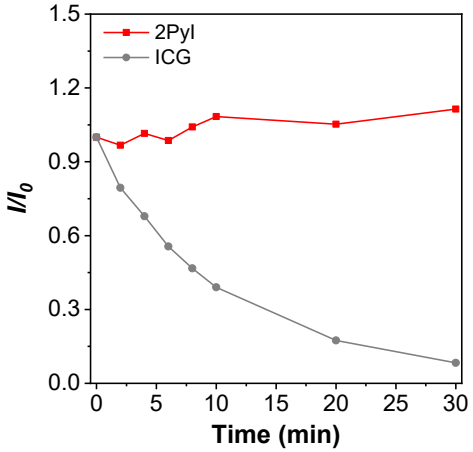

Figure S31. Photostability of 2PyI. Photostability of 2PyI and ICG (10 μM) under continuous laser irradiation at 660 nm (0.1 W cm^{-2}) for 30 min. *I* represents the PL intensity of 2PyI or ICG at different times, while I_0 represents their initial fluorescence intensity at 0 min.

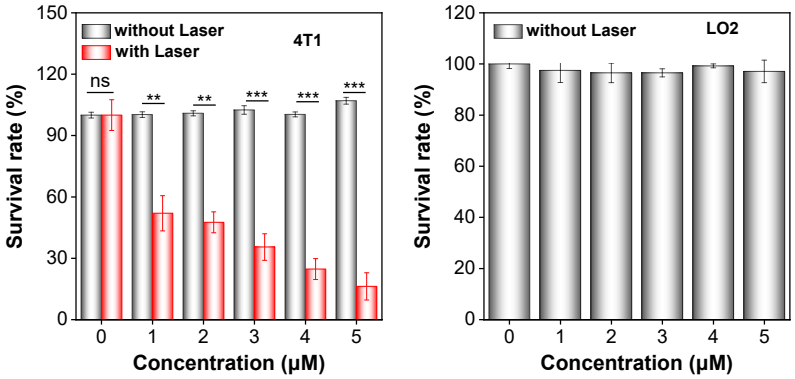

Figure S32. In vitro cytotoxicity assay of 2PyI toward (A) 4T1 cells, (B) LO2 cells with or without 660 nm laser irradiation (0.4 W cm^{-2}, 10 min). Data were presented as mean ± SD (n = 3), $^{**}p<0.01$, $^{***}p<0.001$.

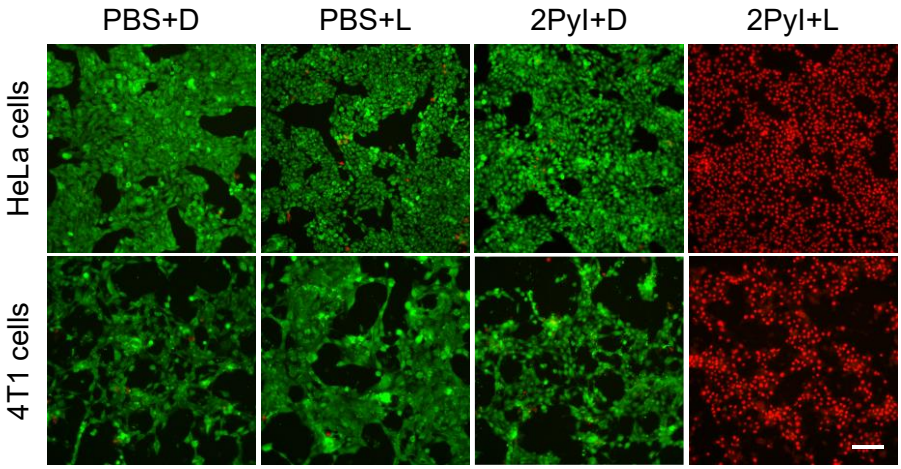

Figure S33. Calcein-AM/PI co-staining imaging of HeLa and 4T1 cells after treated with PBS or 2PyI under 660 nm laser irradiation (0.4 W cm^{-2}, 10 min). Scale bar = 100 μm.

Figure S34. (A) NIR-II fluorescence imaging of major organs and tumor in mice obtained at 72 h after intratumoral injection of 2PyI (1 mM, 100 μL). (B) Relative fluorescence intensity of major organs and tumor. *I* represents the fluorescence intensity of the major organ, while I_H indicates the fluorescence intensity of the heart. Data were presented as mean ± SD (n = 3), $^{***}p<0.001$.

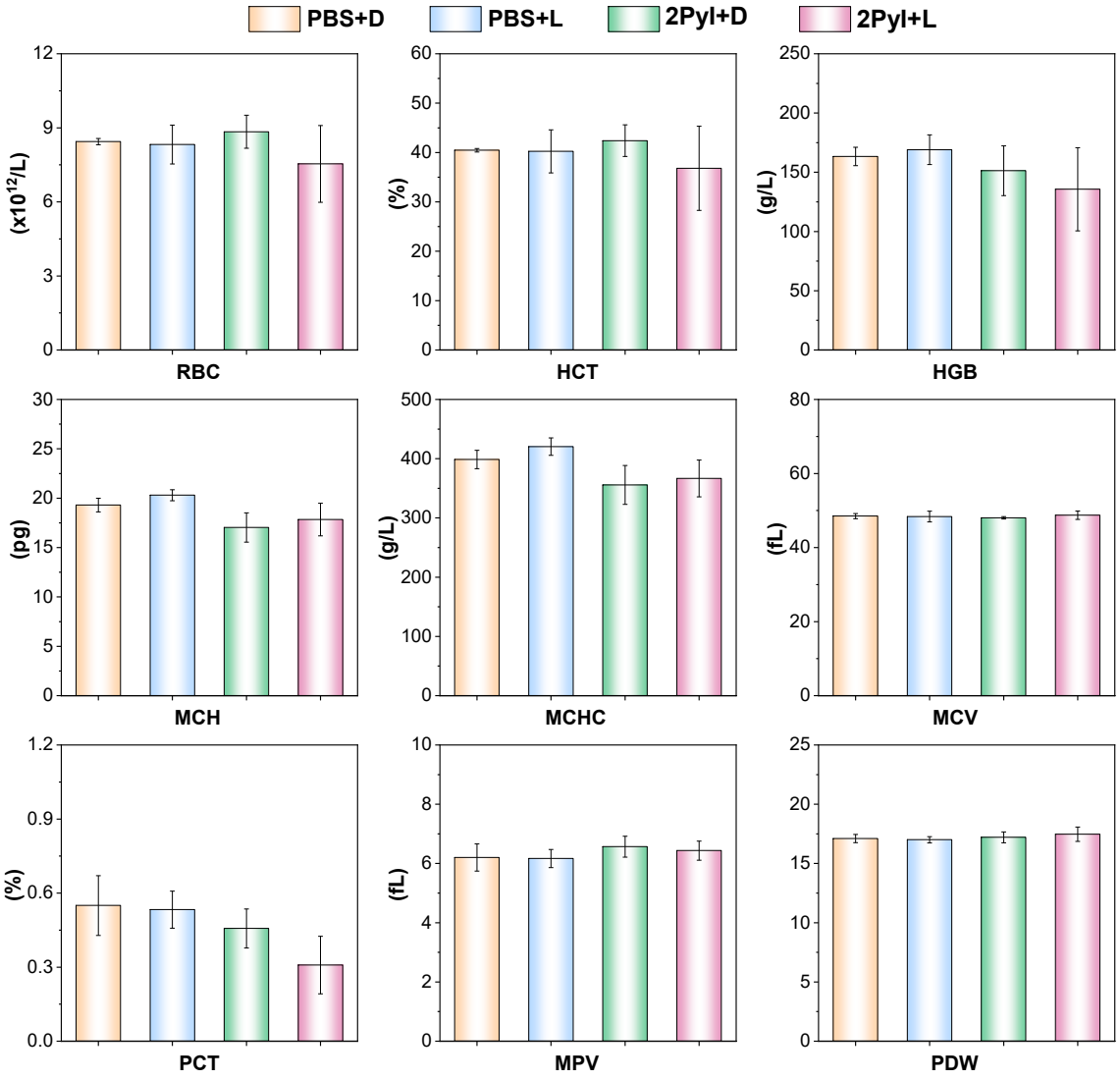

Figure S35. Blood routine assays of mice in different groups. Data were presented as mean ± SD (n = 4).

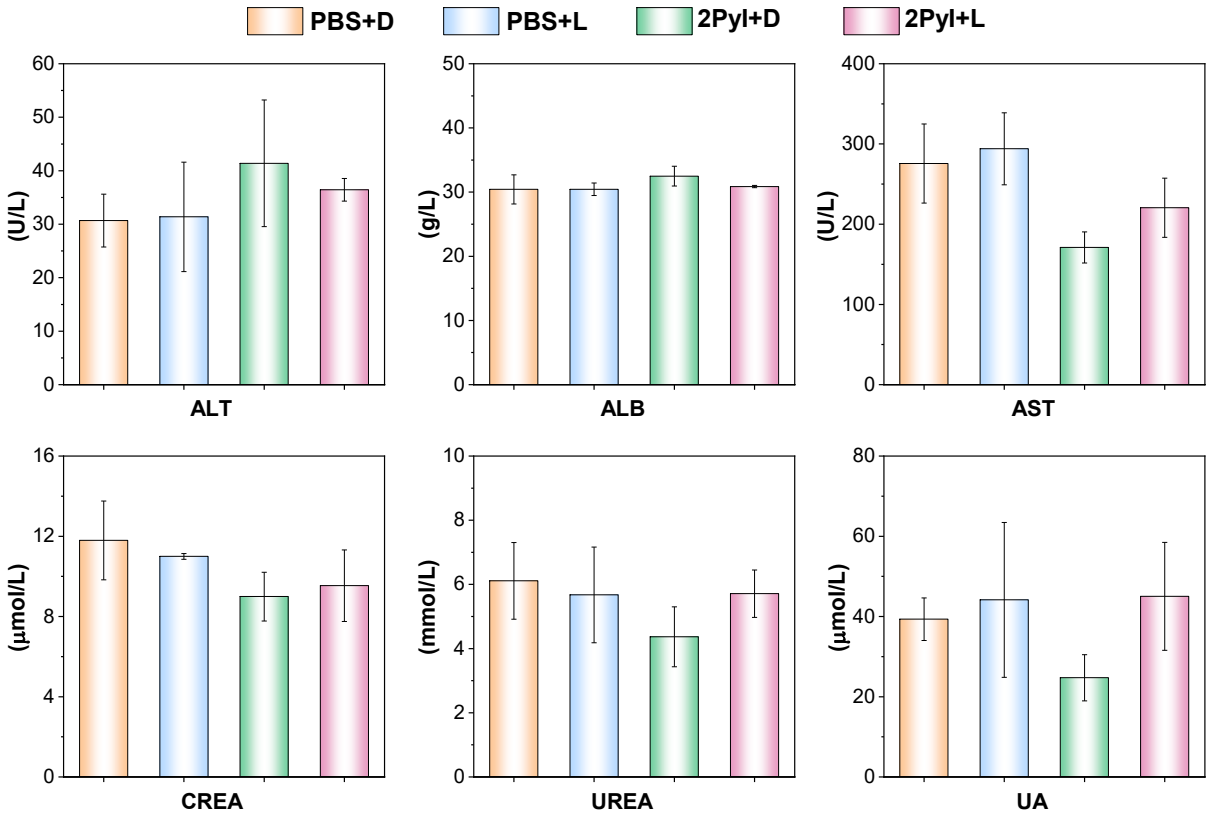

Figure S36. Blood biochemistry test regarding liver and kidney function of the mice in different groups. Data were presented as mean ± SD (n = 4).

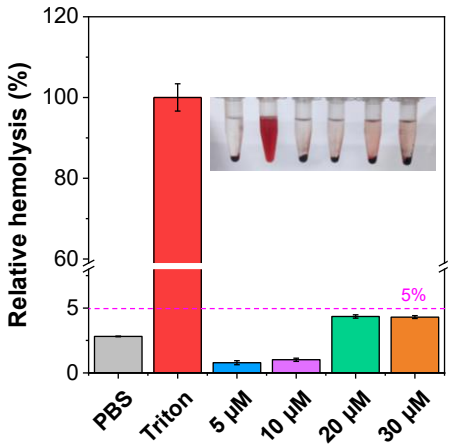

Figure S37. Hemolysis rates of 2Pyl. Triton and PBS were used as the positive control and negative control, respectively. Inset: the photographs of hemolytic activity. Data were presented as mean ± SD (n = 3).

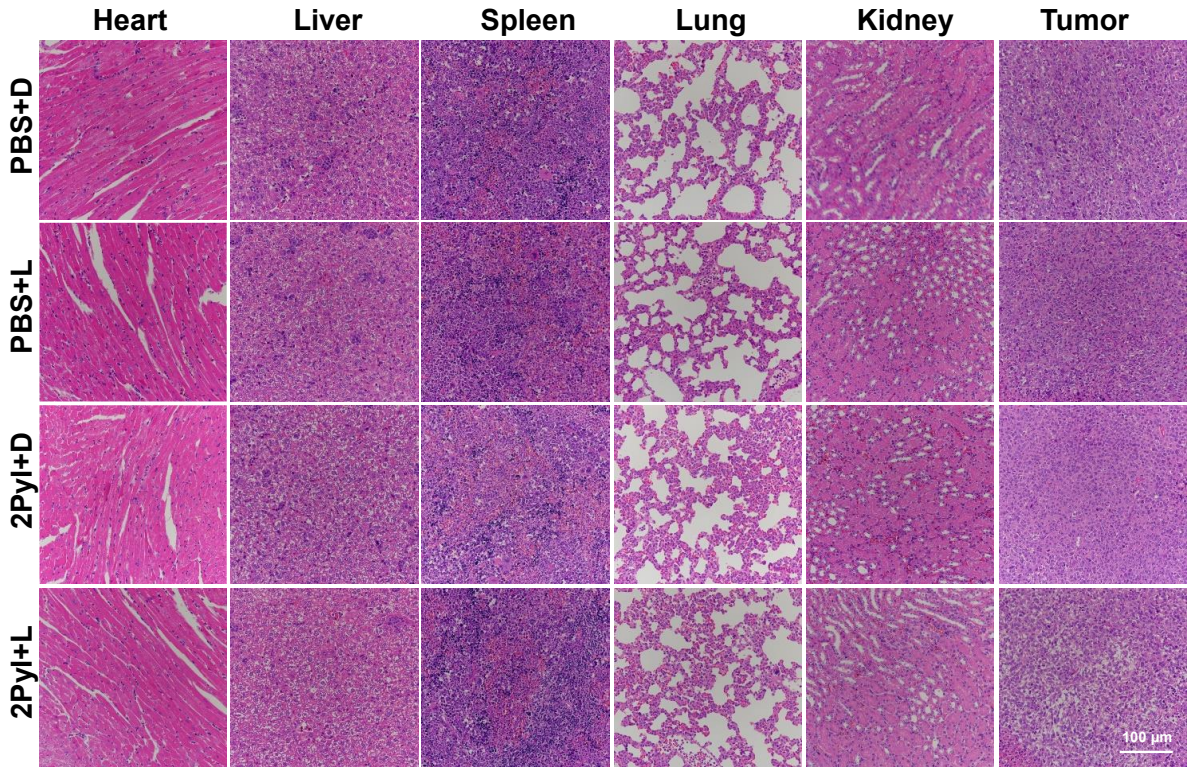

Figure S38. Histological H&E staining of major organs and tumor of mice in different groups.

References

[1] A. Kurutos, Y. Shindo, Y. Hiruta, K. Oka and D. Citterio, *Dyes Pigm.*, 2022, **204**, 110424.

[2] H. J. Zhou and T. B. Ren, *Chem. Asian J.*, 2022, **17**, e202200147.

[3] X. Zhao, H. Zhao, S. Wang, Z. Fan, Y. Ma, Y. Yin, W. Wang, R. Xi and M. Meng, *J. Am. Chem. Soc.*, 2021, **143**, 20828.

[4] T.-T. Zhou, G.-Y. Ding, X. Li, L.-L. Wen, X.-X. Pang, Y.-C. Duan, J.-Y. He, G.-G. Shan and Z.-M. Su, *Chin. Chem. Lett.* 2025, **36**, 110341.

[5] Y. Li, D. Zhang, Y. Yu, L. Zhang, L. Li, L. Shi, G. Feng and B. Z. Tang, *ACS Nano* 2023, **17**, 16993-17003.

[6] J. Zhang, D. Jiao, X. Qi, Y. Zhang, X. Liu, T. Pan, H. Gao, Z. Liu, D. Ding and G. Feng, *Adv. Sci.* 2025, **12**, 2410405.

[7]. J. Zhuang, B. Wang, H. Chen, K. Zhang, N. Li, N. Zhao and B. Z. Tang, *ACS Nano* 2023, **17**, 9110-9125.

[8] M. Guo, Y. Gao, Q. Sun, Z. Wu, R. Ding, K. Zhou, G. He and Y. Zhang, *Sci. China Mater.* 2025, **68**, 4273-4279.

[9] J. Huang, J. Zhu, S. Xiang, L. Wang, D. Wang and B. Z. Tang, *Adv. Funct. Mater.* 2025, **36**, e14187.

[10] X. Chen, L. Shi, X.-Y. Ran, J.-X. Xu, L.-N. Zhang, Q.-Q. Kong, X.-Q. Yu and K. Li, *Adv. Funct. Mater.* 2024, **34**, 2400728.

[11] X. Yang, X. Wang, X. Zhang, J. Zhang, J. W. Y. Lam, H. Sun, J. Yang, Y. Liang and B. Z. Tang, *Adv. Mater.* 2024, **36**, 2402182.

[12] J. Jia, Y. Yu, J. Zhuang, J. Wang, N. Li and N. Zhao, *Chin. Chem. Lett.* 2026, DOI: 10.1016/j.cclet.2026.112428.

[13] Y. Tang, H. K. Bisoyi, X.-M. Chen, Z. Liu, X. Chen, S. Zhang and Q. Li, *Adv. Mater.* 2023, **35**, 2300232.

[14] J. Zhuang, Z. Ma, N. Li, H. Chen, L. Yang, Y. Lu, K. Guo, N. Zhao and B. Z. Tang, *Adv. Mater.* 2024, **36**, 2309488.